Global Biogeochemical Cycles®

RESEARCH ARTICLE
10.1029/2022GB007513

Key Points:

- Two initial-condition large ensembles are used to quantify the ocean physical and biogeochemical response to the eruption of Mt. Pinatubo
- Oxygen is immediately absorbed into the upper ocean and transits to depth where it permanently increases the interior inventory by 60 Tmol
- Mt Pinatubo forced an increase in the ocean carbon sink of -0.29 ± 0.14 Pg C yr^{-1} in 1992

Supporting Information:

Supporting Information may be found in the online version of this article.

Correspondence to:

A. R. Fay,
afay@ldeo.columbia.edu

Citation:

Fay, A. R., McKinley, G. A., Lovenduski, N. S., Eddebbar, Y., Levy, M. N., Long, M. C., et al. (2023). Immediate and long-lasting impacts of the Mt. Pinatubo eruption on ocean oxygen and carbon inventories. *Global Biogeochemical Cycles*, *37*, e2022GB007513. https://doi.org/10.1029/2022GB007513

Received 30 JUN 2022
Accepted 20 JAN 2023

Immediate and Long-Lasting Impacts of the Mt. Pinatubo Eruption on Ocean Oxygen and Carbon Inventories

Amanda R. Fay[1], Galen A. McKinley[1], Nicole S. Lovenduski[2,3], Yassir Eddebbar[4], Michael N. Levy[5], Matthew C. Long[5], Holly C. Olivarez[3,6], and Rea R. Rustagi[1]

[1]Lamont-Doherty Earth Observatory, Columbia University, Palisades, NY, USA, [2]Department of Atmospheric and Oceanic Sciences, University of Colorado, Boulder, CO, USA, [3]Institute of Arctic and Alpine Research, University of Colorado, Boulder, CO, USA, [4]Scripps Institution of Oceanography, University of California San Diego, La Jolla, CA, USA, [5]Climate and Global Dynamics Laboratory, National Center for Atmospheric Research, Boulder, CO, USA, [6]Department of Environmental Studies, University of Colorado, Boulder, CO, USA

Abstract Large volcanic eruptions drive significant climate perturbations through major anomalies in radiative fluxes and the resulting widespread cooling of the surface and upper ocean. Recent studies suggest that these eruptions also drive important variability in air-sea carbon and oxygen fluxes. By simulating the Earth system using two initial-condition large ensembles, with and without the aerosol forcing associated with the Mt. Pinatubo eruption in June 1991, we isolate the impact of this volcanic event on physical and biogeochemical properties of the ocean. The Mt. Pinatubo eruption forced significant anomalies in surface fluxes and the ocean interior inventories of heat, oxygen, and carbon. Pinatubo-driven changes persist for multiple years in the upper ocean and permanently modify the ocean's heat, oxygen, and carbon inventories. Positive anomalies in oxygen concentrations emerge immediately post-eruption and penetrate into the deep ocean. In contrast, carbon anomalies intensify in the upper ocean over several years post-eruption, and are largely confined to the upper 150 m. In the tropics and northern high latitudes, the change in oxygen is dominated by surface cooling and subsequent ventilation to mid-depths, while the carbon anomaly is associated with solubility changes and eruption-generated El Niño—Southern Oscillation variability. We do not find significant impact of Pinatubo on oxygen or carbon fluxes in the Southern Ocean; but this may be due to Southern Hemisphere aerosol forcing being underestimated in Community Earth System Model 1 simulations.

Plain Language Summary The eruption of Pinatubo in June of 1991 produced sunlight-reflecting aerosols in the upper atmosphere and led to a cooling of the planet for several years. While the global cooling following the eruption is well documented, the impact of the eruption on the ocean oxygen and carbon budgets has received comparably little attention. As the global ocean oxygen concentration is declining in response to climate change, and as the ocean's continued storage of anthropogenic carbon is critical for the climate system, it is of interest to quantify the effect of the eruption on both oxygen and carbon in the global ocean. Here, we use an Earth system model to simulate the historical evolution of the climate system both with and without the Mt. Pinatubo eruption. By comparing the simulations, we are able to quantify the effect of the eruption on ocean properties. We find that the eruption led to cooler surface ocean temperatures, and increases in the ocean oxygen and carbon concentrations that persisted for many years. Our simulations can also be used to study other Earth system changes caused by the eruption.

1. Introduction

As a result of anthropogenic activities, the global ocean is losing oxygen and gaining carbon. Observations indicate that the ocean's oxygen inventory has declined by about 2% in the 5 decades following 1960 as the upper ocean warms and stratifies (Ito et al., 2017; Schmidtko et al., 2017). This oxygen loss has major consequences for nutrient cycling, compression of marine ecosystem habitats, and global fisheries (Deutsch et al., 2015; Gruber, 2011; Keeling et al., 2010). Since pre-industrial times, the ocean has absorbed ~170 Pg of anthropogenic carbon from the atmosphere (Canadell et al., 2021), which is beneficial for the mitigation of anthropogenic warming, but harmful to some organisms through the related decline in pH, known as ocean acidification.

These long-term changes in ocean oxygen and carbon are superimposed on large interannual to multi-decadal variability, challenging the attribution of reported trends (Long et al., 2016; McKinley et al., 2016; Schlunegger et al., 2020). Due to their sensitivity to physical and biogeochemical processes, ocean oxygen concentrations and

air-sea fluxes exhibit substantial variability across a range of timescales in observations and models (Deutsch et al., 2011; Eddebbar et al., 2017; Ito et al., 2010; McKinley et al., 2003). Modeling and observation-based studies suggest that both air-sea carbon dioxide flux and ocean carbon concentrations exhibit variability on interannual to multi-decadal timescales (DeVries et al., 2017; Gruber et al., 2019; Resplandy et al., 2015). Many studies highlight internal climate processes and modes of variability (e.g., El Niño—Southern Oscillation [ENSO], North Atlantic Oscillation [NAO], Pacific Decadal Oscillation [PDO], Southern Annular Mode [SAM]) as major drivers controlling variations in the fluxes and inventories of global ocean oxygen and carbon (Deutsch et al., 2011; Eddebbar et al., 2017; Gruber et al., 2019; Ito & Deutsch, 2013; Landschützer et al., 2016, 2019; Lovenduski et al., 2007; McKinley et al., 2003, 2004, 2017). Others suggest an important role for externally driven climate perturbations (e.g., volcanic eruptions) in contributing to these variations (Eddebbar et al., 2019; Frölicher et al., 2009, 2011, 2013; McKinley et al., 2020). It is critical that we develop a fundamental understanding of the drivers of past ocean oxygen and carbon variability so as to allow for clear interpretation of the observational record and also we can more confidently predict future change.

Despite their well-known influence on global and regional climate (Marshall et al., 2022) and ocean heat uptake (Gupta & Marshall, 2018), the impact of volcanic eruptions on ocean biogeochemistry is not well quantified. The explosive eruption of the Pinatubo stratovolcano in the Philippines on 15 June 1991 was the largest in the last 100 years. The volcanic release of sulfur dioxide and subsequent aerosol interactions in the stratosphere led to a substantial scattering of shortwave irradiance and a major reduction in solar heating at the sea surface, driving persistent global and regional changes in climate (Dutton & Christy, 1992; Marshall et al., 2022). The subsequent cooling effect from eruptions of this magnitude have the potential to cause a dramatic, though temporary, pause in global warming trends (Church et al., 2005; Robock & Mao, 1995). The eruption immediately preceded a boom in ocean observations occurring with the World Ocean Circulation Experiment (WOCE) and Joint Global Ocean Flux Study (JGOFS) (Gould et al., 2013). Thus, it is possible the impacts from Pinatubo have been imprinted in these observations.

Past studies suggest that volcanic-induced climate perturbations can have a profound influence on the oceanic oxygen and carbon distributions and air-sea fluxes. Using a model ensemble, Frölicher et al. (2009) found that volcanic eruptions lead to an increase in interior ocean oxygen concentrations, with volcanic anomalies in oxygen gradually penetrating the top 500 m of the ocean and persisting for several years, but with considerable interannual to decadal variability. However, the small number of ensemble members (three members) used in their study made regional attribution and process understanding of volcanic effects difficult due to confounding effects of internal (unforced) climate variability. A more recent modeling study leveraged the large number of ensemble members from the Community Earth System Model (CESM) and Geophysical Fluid Dynamics Laboratory model (GFDL) Large Ensembles (LENS) experiments to explore the volcanic effects from eruptions occurring since 1950 (Eddebbar et al., 2019). They found that tropical eruptions generate strong and spatially decoupled ocean oxygen and carbon uptake, suggesting different processes at play throughout the ocean regions. The simulated oceanic oxygen uptake associated with the eruptions of Agung (1963), El Chichon (1982), and Pinatubo (1991) occurred primarily at mid and high latitudes and acted to reduce the magnitude of global ocean deoxygenation due to anthropogenic warming. This study also showcased strong carbon uptake at lower latitudes associated with an El Niño-like response to tropical eruptions in the tropical Pacific that is common across Earth system models (McGregor et al., 2020). While the large number of ensemble members substantially reduced the confounding influence of internal variability, the combined effect of various external forcings (anthropogenic greenhouse gases, industrial aerosols, and volcanic aerosols) in this study challenges direct attribution and isolation of volcanic eruption effects on prolonged timescales.

In this study, we conduct numerical experiments that isolate the ocean's response to the volcanic forcing, so as to more clearly assess long-term deoxygenation trends and understand variations in carbon uptake and storage attributable to the Mt. Pinatubo eruption. We quantify the impacts of the Pinatubo eruption on ocean concentrations and air-sea fluxes of oxygen and carbon, and place them into context with anthropogenic forced changes and internally driven climate variability. While this paper is limited in scope to an introduction of the model experiments and the examination of oxygen and carbon impacts in the ocean, scientists throughout the community will find benefit from these runs for understanding the impact of Pinatubo throughout the climate system.

Here, the combined analysis of oxygen and carbon changes presents a unique and complementary perspective on how ocean biogeochemistry and circulation respond to large scale radiative perturbations. Our tool for assessment

of the impacts of Pinatubo is a set of large initial condition ensembles of the CESM Large Ensemble (CESM-LE) experiment Kay et al. (2015), where each ensemble member has different phasing of internal climate variability. For our study, the first ensemble is forced with historical and projected future external forcing, while the second ensemble is forced identically with the sole exception that it excludes the aerosols due to the Pinatubo eruption. This experimental protocol permits a clean separation of the climate and biogeochemical impacts of the Pinatubo eruption on the Earth system.

First we will introduce the model setup experiments for this work including some validation of the CESM model. In Section 3, we evaluate the global mean and spatial patterns of the difference between these two ensembles for SST, oxygen and carbon air-sea exchanges and inventories. We consider these as indicators of the impact of the eruption on the ocean's physical and biogeochemical state. In Section 4, we discuss the mechanisms behind these changes, relationships to climate modes, and consider comparisons to observations and previous modeling work on the topic. Thoughts on the direction for future work are also included here. We conclude in Section 5 with a summary of our results.

2. Methods

To generate an initial-condition large ensemble, a climate model is run multiple times under identical forcing, but with very small perturbations in initial conditions. These perturbations evolve naturally and amplify rapidly, such that each ensemble member follows a unique climate trajectory through the phase space. The external forcing response, associated with the shared identical external forcing, is isolated when taking the mean across the ensemble. Within the framework of NCAR's CESM-LE effort (Kay et al., 2015), we develop a new experiment with 29 members for 1990–2025 that explicitly excludes the forcing from Pinatubo (CESM-LE-NoPin). We are then able to isolate the externally forced response due to the volcanic eruption through a comparison between these two ensembles. The forced effect due to Pinatubo is quantified as the difference between the mean of 29 CESM-LE-NoPin ensemble members and the mean of the 29 CESM-LE members from which these were branched off. This forced effect is not directly observable in the real world. Instead, real world observations are akin to a single ensemble member that includes both the forced signal and internal variability (Deser, Phillips, Bourdette, & Teng 2012; Deser, Knutti, Solomon, & Phillips 2012). The ensemble members analyzed here are not initiated with observed climate states and are thus not expected to simulate real-world observed climate in their mean response. Instead, each member of the ensemble is a potential evolution of the Earth's climate that emerges from the coupled interactions of the atmosphere-ocean-cryosphere-land system. Results from Large Ensemble experiments such as CESM-LE show substantial influence of internal climate variability on twentieth- to twenty-first-century climate trajectories (Kay et al., 2015).

As a coupled climate model, each ensemble member of CESM-LE develops its own phasing of internal variability that does not necessarily correspond with the phasing in the real world observations. This internal climate variability is known to affect climate projections, however its influence is often underappreciated and confused with model error. Scientists use CESM-LE and other large ensemble output to help interpret the observational record, to understand projection spread, and to consider the range of possible futures influenced by both internal climate variability and forced climate change (Deser, Phillips, Bourdette, & Teng 2012; Deser, Phillips, Tomas, et al., 2012; Deser et al., 2020; Kay et al., 2015; McKinley et al., 2016, 2017). In this experiment, the spread across the ensemble indicates the potential magnitude of the Earth system response to Pinatubo across multiple realizations of internal variability. Considering both the forced response and the internal spread, we evaluate the near-term and long-term interior ocean carbon and oxygen effects of Pinatubo, and connect these changes to surface flux patterns. Where appropriate, we place the forced changes and ensemble spread into context with observed changes in the ocean.

2.1. The Community Earth System Model

We use the CESM version 1 (CESM1; Hurrell et al., 2013) to conduct our large ensemble simulations. CESM1 consists of atmosphere, ocean, land, and sea ice component models (Danabasoglu et al., 2012; Holland et al., 2012; Hunke & Lipscomb, 2008; Lawrence et al., 2012). The coupled atmospheric model is the Community Atmospheric Model version 5 (CAM5), integrated at nominal 1° horizontal resolution with 30 vertical levels (Hurrell et al., 2013). Volcanic radiative forcing is incorporated in the CESM-LE using the forcing data set of Ammann et al. (2003). Stratospheric aerosol in CESM1-CAM5 is treated by prescribing a single, zonally averaged species.

The prescription consists of a monthly mean mass distributed on a predefined meridional and vertical grid (Neely III et al., 2016). This aerosol mass is assumed to be comprised of 75% sulfuric acid and 25% water and to have a constant log-normal size distribution.

The ocean physical model, Parallel Ocean Program, version 2 (Smith et al., 2010) has nominal 1° horizontal resolution and 60 vertical levels. Mesoscale eddy transport, diapycnal mixing, and mixed layer restratification by submesoscale eddies are parameterized with state-of-the-art approaches (Danabasoglu et al., 2020). The biogeochemical-ecosystem ocean model, known as the Biogeochemical Elemental Cycling (BEC) model, includes multi-nutrient co-limitation on phytoplankton growth and specific phytoplankton functional groups as well as full-depth ocean carbonate system thermodynamics, sea-to-air O_2, and CO_2 fluxes, and a dynamic iron cycle (Moore et al., 2013).

While direct comparisons to observations are challenging given the set-up of a Large Ensemble ESM, CESM has a proven track record of performing well on many physical and biogeochemical variables. A comparison of the CESM-LE mean Atlantic Meridional Overturning Circulation (AMOC) to observations from the RAPID array are well within the uncertainty bounds; observations from the array at 26.5 N report a long term mean for years 2004–2017 of 17.0 $\pm$ 3.1 Sv (2σ) (Smeed et al., 2018) while the model has a mean of 19.97 Sv. It is important to note though that the years covered by the observations are mostly in the timeframe of the model that is following the RCP8.5 pathway so differences are not unexpected. Observations of AMOC prior to 2004 are not available.

Much previous work has been published comparing the CESM model to observations, therefore providing confidence in our results. While there are many factors that limit the ability of a model to accurately capture observed variability, including coarse model resolution, model drift, and mean-state biases, previous work shows that the CESM-LE model is a useful tool to consider changes such as those discussed here. Eddebbar et al. (2019) consider modeled Atmospheric Potential Oxygen and CO_2 fluxes in the context of observed natural variability, and also evaluate fluxes from a hindcast simulation of CESM (Long et al., 2013) which simulates the expected ocean biogeochemical response (oxygen and carbon fluxes) to observed atmospheric conditions. The biogeochemical-ecosystem model compares favorably to observations, though there are some important known biases, including weak Southern Ocean CO_2 uptake (Long et al., 2013). CESM also exhibits Oxygen Minimum Zones that are more pronounced than observations (Long et al., 2016), particularly over the tropical Pacific where inadequate ventilation by the equatorial undercurrent and mesoscale eddies are poorly simulated at the coarse 1° nominal resolution (Busecke et al., 2019; Cabré et al., 2015; Eddebbar et al., 2021) (Figure S12 in Supporting Information S1). Long et al. (2016) discuss comparisons between dissolved oxygen levels in CESM-LE and WOA and find the observed large-scale spatial pattern of oxygen to be well represented by CESM; negatively biased model oxygen is widespread in the tropics where oxygen minimum zones in the model are too extensive, which could be attributable to sluggish circulation yielding weak ventilation. Additionally, they find that the model's western North Pacific is strongly deficient in oxygen, likely due in part to a poor representation of diapycnal mixing over rough topography.

While these biases exist in the model, our analysis focuses on the anomaly between two large ensemble runs from this model, so biases in the mean state are likely to be much reduced and thus are not considered in this analysis. It is possible that the internal variability of the model, which is the focus of this work, could be impacted by these mean biases via nonlinear feedbacks. Biases in CESM1 associated with the depth of the climatological thermocline are known to influence ENSO predictions both in magnitude and pattern (Wu et al., 2022). We thus expect that biases in the mean distribution and variability of temperature, oxygen, and carbon may potentially lead to different eruption responses in the model than observations. The impacts of these biases and direct comparison to observations are left to future study. Future work running similar large ensemble set ups by other modeling groups would be ideal in strengthening our understanding of this impact of Pinatubo and we hope this work inspires such collaboration efforts.

2.2. CESM No Pinatubo Experiment (CESM-LE-NoPin)

The CESM-LE-NoPin setup is identical to the CESM-LE setup, but excludes the effect of the eruption by adjusting the volcanic aerosol mass mixing ratio within the model. Specifically, the volcanic aerosol mass mixing ratio values in CESM-LE-NoPin for January 1991 to December 1995 were replaced with values from January 1986 to December 1990 to simulate a time without impact from volcanic eruptions. Since Pinatubo was the dominant climatically important volcano during this period, we attribute the resulting climatic and ocean biogeochemical

changes to Pinatubo. With this single change in the model setup, we are capturing effects attributable to the physical climate anomalies, however the methodology utilized in this model set up does not consider impacts from volcanic dust deposition on biomass production or other secondary feedbacks on the ocean from volcanic eruptions (Hamme et al., 2010).

Conceptually, the CESM-LE-NoPin ensemble can be thought of as multiple realizations from a "control" climate that did not experience Pinatubo, while the original CESM-LE can be thought of as an "experiment" where each realization, or ensemble member, includes the eruption. We ran the 29 ensemble members of CESM-LE and CESM-LE-NoPin on the same supercomputer (NCAR Cheyenne) to avoid differences in output generated by machine and compiler changes; the original CESM-LE was run on NCAR's Yellowstone machine.

2.3. Statistical Analysis

We present Pinatubo-driven anomalies throughout the manuscript, where anomalies represent the difference between the CESM-LE and the CESM-LE-NoPin output. We quantify the forced impact of the eruption as the difference between the CESM-LE and CESM-LE-NoPin ensemble means (X). The internal variability is defined as the standard deviation (σ) across the ensemble members anomalies (CESM-LE minus CESM-LE-NoPin) at each time step. Analysis is conducted on a monthly model output.

The forced impact of the eruption is statistically significant at the 95% confidence level (Deser, Phillips, Bourdette, & Teng 2012), if its ratio of the ensemble mean difference (X) with the internal spread (σ) is greater than 2 divided by the square root of the degrees of freedom ($N-1$; here $N=29$),

$$\frac{X}{\sigma} \geq \frac{2}{\sqrt{N-1}}. \tag{1}$$

When considering annual mean anomalies for the years following the eruption (Figures 4 and 5), we use July as the first month of each year to ensure symmetry around the peak of ENSO. Consistent with previous work on the topic (Eddebbar et al., 2019), we refer to the 12 months following the eruption as Year 0 (July 1991–June 1992), and subsequent years as Year 1 (July 1992–June 1993), Year 2 (July 1993–June 1994), etc.

3. Results

Oxygen and carbon in the ocean are sensitive to a number of different physical processes in the climate system. In this section, we briefly describe the eruption-driven changes in ocean temperature, heat content, mixed layer depth, and circulation that are relevant for oxygen and carbon. We then perform a detailed investigation of the oxygen and carbon anomalies driven by Pinatubo.

3.1. Physical Response to Pinatubo

The eruption of Pinatubo in June of 1991 drives an immediate reduction in global mean sea surface temperature (SST) followed by a prolonged recovery (Figure 1a). The forced SST anomaly due to Pinatubo reaches a maximum of 0.18°C 1 year post-eruption, with a statistically significant cooling anomaly persisting for 5 years post eruption, despite an ensemble spread of ±0.08°C (Figure 1b). Below the sea surface, Pinatubo leads to a substantial heat loss, reaching a maximum of -3.5×10^{22} J across the entire water column by mid-1993, with most of this heat loss occurring in the upper 250 m (Figures 2a, 2b, and 3a). A globally averaged vertical profile Hovmöller plot of the difference of the two ensemble means (CESM-LE minus CESM-LE-NoPin) shows that significant cooling begins in 1992 for the upper ocean, with global-mean anomalies as large as 0.2°C penetrating down to 150 m (Figure 3a). Smaller, but still significant, anomalies persist to depths below 1,000 m. Ocean heat content (OHC) remains significantly altered by the eruption at the 95% confidence level through the year 2000 for the 250 m inventory and persists longer for full depth inventories (Figure 2b). Below 1,000 m, the Pinatubo effect on heat content remains statistically significant for the duration of our experiments that end in 2025 (-2×10^{22} J, Figure S1 in Supporting Information S1), while the upper 250 m rebounds toward a heat content statistically indistinguishable from CESM-LE-NoPin after 2004 (Figure 2b). While there is some recovery in the two years following the maxima anomaly in OHC, the recovery stops quite abruptly in 1996 for all depths, and only modest changes are seen in the anomalies after that year, specifically at depths below 250 m (Figure 2b). Our results

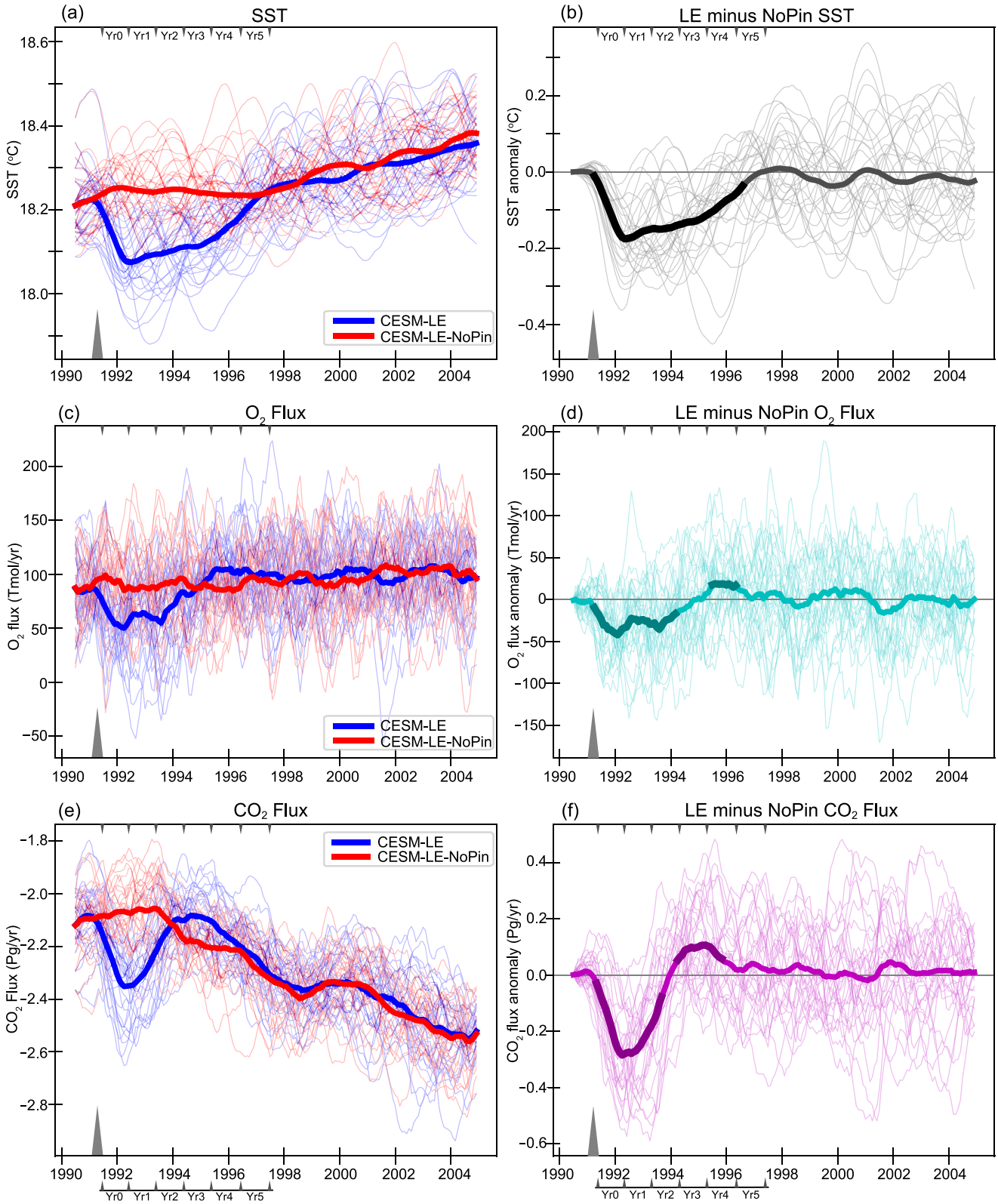

Figure 1. Left column: Community Earth System Model Large Ensemble (CESM-LE) (blue) and CESM-LE-NoPin (red) individual members (thin lines) and ensemble mean (thick line) time series for global mean sea surface temperature (top, °C), Oxygen flux (middle, Tmol yr^{-1}), and CO_2 Flux (bottom, Pg yr^{-1}) for 1990–2004. Right column: CESM-LE minus CESM-LE-NoPin difference for each variable with thicker line indicating significant difference between the two ensembles at 2σ (Deser, Phillips, Bourdette, & Teng 2012). Time series are seasonally detrended and smoothed with a 12-month running mean. Gray triangles mark timing of eruption. Full time series through 2025 available in Figure S1 in Supporting Information S1.

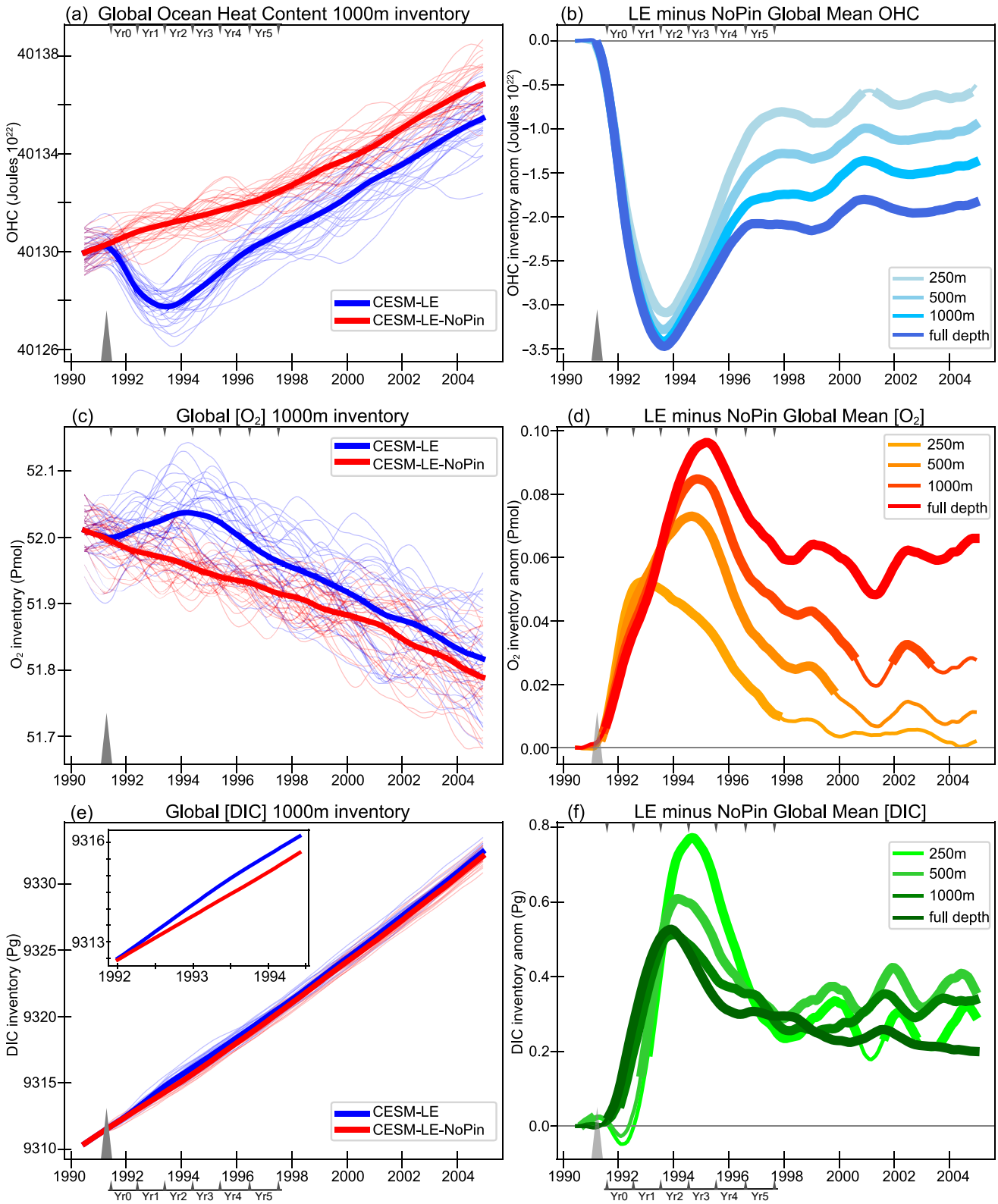
(a) Global Ocean Heat Content 1000m inventory
OHC (Joules 10^22)
CESM-LE
CESM-LE-NoPin
(b) LE minus NoPin Global Mean OHC
OHC inventory anom (Joules 10^22)
250m
500m
1000m
full depth
(c) Global [O2] 1000m inventory
O2 inventory (Pmol)
(d) LE minus NoPin Global Mean [O2]
O2 inventory anom (Pmol)
(e) Global [DIC] 1000m inventory
DIC inventory (Pg)
(f) LE minus NoPin Global Mean [DIC]
DIC inventory anom (Pg)
Yr0 Yr1 Yr2 Yr3 Yr4 Yr5

Figure 2.

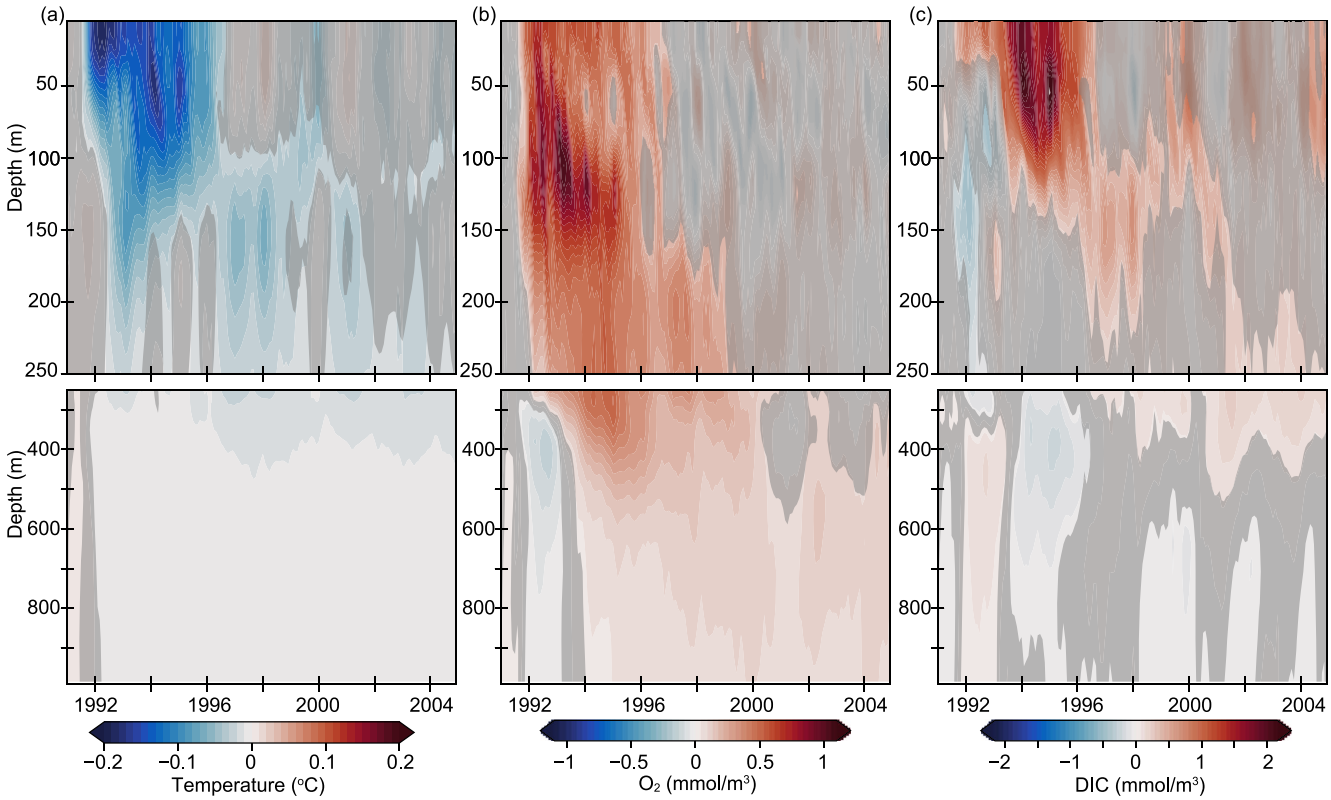

Figure 3. Globally averaged vertical profile of difference plots (Community Earth System Model Large Ensemble [CESM-LE] minus CESM-LE-NoPin) for ensemble mean in (a) temperature (°C) (b) (O_2) (mmol m^{-3}), and (c) (DIC) (mmol m^{-3}). Shading indicates time/depth where differences are not significant at the 95% confidence level (Deser, Phillips, Bourdette, & Teng 2012). Positive anomalies (warm colors) indicate greater values with the eruption of Pinatubo while negative anomalies (cool colors) indicate lower values with the eruption. Full model time period available in Figure S3 in Supporting Information S1.

show that Pinatubo causes a net heat loss that is not recovered even 3 decades after the eruption, consistent with previous modeling work (Frölicher et al., 2011).

Spatial features of SST anomalies show that Pinatubo-driven cooling is concentrated in the tropics in the year immediately following the eruption (Figure 4, left, Year 0). Cooling quickly spreads over much of the surface ocean by Year 1 (1992–1993) with significant anomalies, given the spread of internal variability indicated by the model ensemble, throughout much of the Pacific basin (unshaded areas in Figure 4). In Year 1 there is also warming surface temperatures in the eastern equatorial Pacific, indicating the development of an El Niño event (Figure S4 in Supporting Information S1). In Year 2 (1993–1994), this switches to a forced tendency to La Niña patterns in the equatorial Pacific, while northern hemisphere forced reductions in SST continue. In Year 3 (1994–1995), the forced tendency to La Niña is the primary Pinatubo-driven cooling signal that persists. By Year 4 (1995–1996), the forced surface cooling has largely dissipated, with internal variability masking any significant signal in the anomalies. Throughout the first 5 years post eruption (Year 0–4), no statistically significant cooling is simulated in the Southern Ocean. The Pacific sector of the Southern Ocean shows the strongest forced signal anomalies, although not emerging from the spread of internal variability, with warming during Year 0 and 1 followed by a cooling in subsequent years. These spatial maps (Figure 4) indicate that the global-mean evolution of temperatures (Figure 3a) is initially dominated by the Northern extratropics and then by a multi-year tendency to La Niña conditions in the equatorial Pacific.

Figure 2. Left column: Community Earth System Model Large Ensemble (CESM-LE) (blue) and CESM-LE-NoPin (red) individual members (thin lines) and ensemble mean (thick line) time series for global mean Ocean Heat Content (top, Joules 10^{22}), Oxygen inventory (middle, Pmol), and Dissolved Inorganic Carbon inventory (bottom, Pg) for top 1,000 m. Inset on DIC inventory (bottom, left) shows a zoomed in ensemble mean time series for 1992–1995 to highlight the difference post eruption. Right column: CESM-LE minus CESM-LE-NoPin inventory difference for each variable with thicker line indicating significant difference between two ensembles at 2σ (Deser, Phillips, Bourdette, & Teng 2012). Inventory plots include lines for depths 250, 500, 1,000 m, and full depth. Time series are seasonally detrended, smoothed with a 12-month running mean. Gray triangle marks timing of eruption. Full time series through 2025 available in Figure S2 in Supporting Information S1.

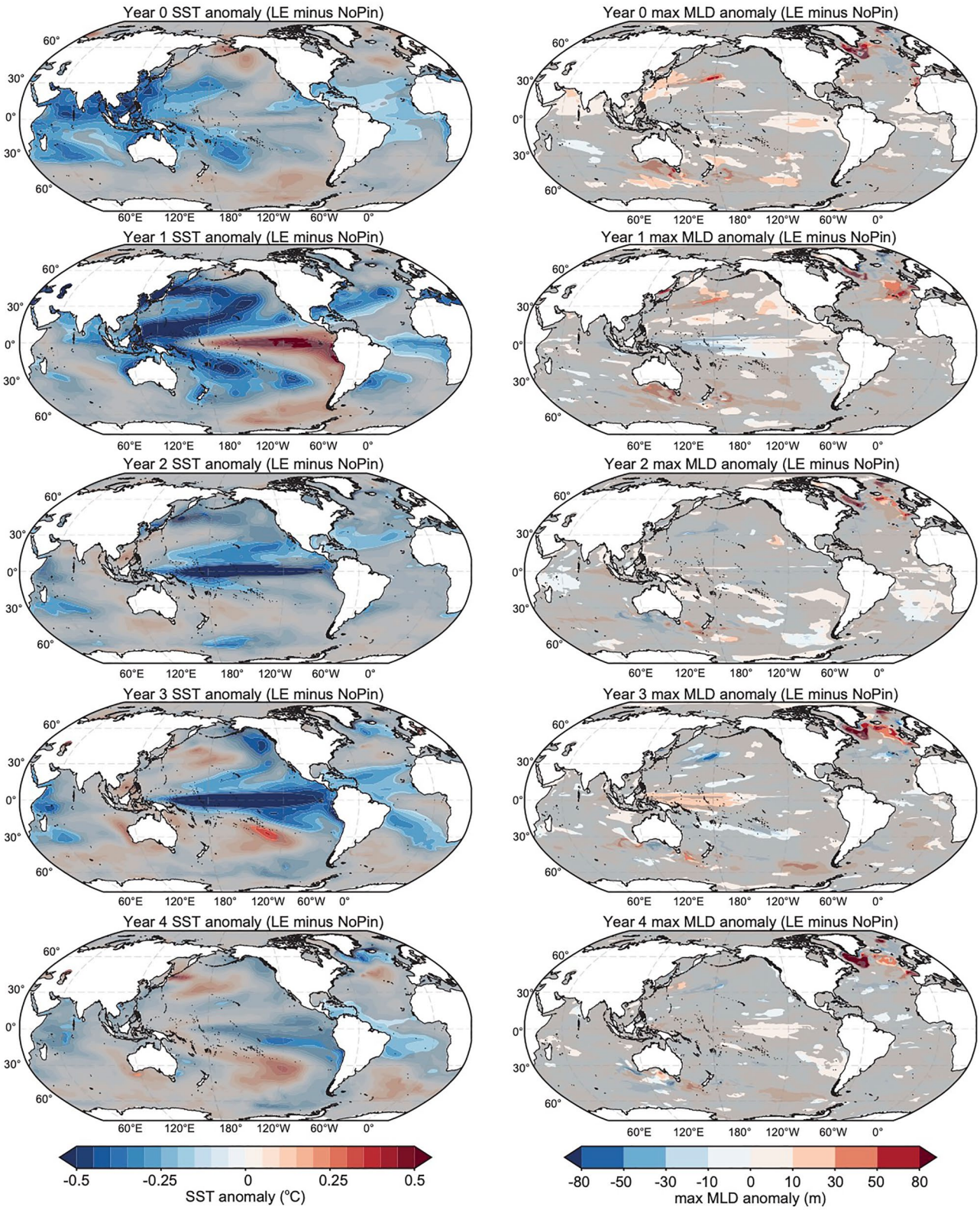
Year 0 SST anomaly (LE minus NoPin)
Year 0 max MLD anomaly (LE minus NoPin)
Year 1 SST anomaly (LE minus NoPin)
Year 1 max MLD anomaly (LE minus NoPin)
Year 2 SST anomaly (LE minus NoPin)
Year 2 max MLD anomaly (LE minus NoPin)
Year 3 SST anomaly (LE minus NoPin)
Year 3 max MLD anomaly (LE minus NoPin)
Year 4 SST anomaly (LE minus NoPin)
Year 4 max MLD anomaly (LE minus NoPin)
60°E 120°E 180° 120°W 60°W 0°
60° 30° 0° 30° 60°
-0.5 -0.25 0 0.25 0.5
SST anomaly (°C)
-80 -50 -30 -10 0 10 30 50 80
max MLD anomaly (m)

Figure 4.

Significant forced changes in maximum mixed layer depths (maxMLD) are spatially patchy, but do occur in extratropical locations important to upper and deep ocean ventilation (Figure 4, right). In the North Atlantic subpolar region across Years 0–4, there are some patches of significant forced maxMLD increases, particularly in the eastern gyre and in the Labrador and Irminger Seas. In the North Pacific, mode water regions experience significant forced increase in maxMLD in Year 0 and 1, and some forced decline in Year 4. Only weak forced change in maxMLD anomalies occur in scattered locations throughout the Southern Ocean.

3.2. Oxygen and Carbon Response to Pinatubo

The physical changes in temperature and circulation following Pinatubo are accompanied by pronounced changes in carbon and oxygen distributions and fluxes (Figures 1 and 2). The forced oxygen flux anomaly peaks at -42 Tmol yr^{-1} in 1992 (negative indicating a net flux into the ocean), with an ensemble spread (σ) of ± 31.5 Tmol yr^{-1} (Figures 1c and 1d). The forced carbon flux anomaly reaches -0.29 Pg C yr^{-1} in 1992, with an ensemble spread ± 0.14 Pg C yr^{-1} (Figures 1e and 1f). The ensemble mean anomaly in O_2 and CO_2 flux is robust at the 95% confidence level with the forced response of these fluxes persisting through 1996 (Figures 1d and 1f). The global mean fluxes are large initially after the eruption due to the cooling of the surface ocean, but then the increased uptake weakens and rebounds to a significant forced reduction in the flux in years 1994–1996 as temperatures rebound (Figure 1, left column).

Oxygen and carbon inventory in the top 1,000 m for both ensembles illustrate significant perturbations amid a backdrop of decreasing and increasing long-term trends, respectively (Figures 2c and 2e). The oxygen inventory time series reflects the global deoxygenation trend, with a clear divergence between the ensemble means of the CESM-LE and CESM-LE-NoPin experiments (Figure 2c). The anomalous oxygen uptake by the oceans immediately following the eruption (Figures 1c and 1d) causes an increase in the O_2 content that is strong enough to temporarily counteract the effects of ocean deoxygenation. This pause in the deoxygenation trend extends through 1995 before the decline resumes (Figure 2c). The modeled collective change in surface oxygen fluxes over years 1991–1996 is -77.5 Tmol (or -0.0775 Pmol) which is reflected in the increase in oxygen inventory in the upper 500 m during that same time frame (Figure 2d).

There are significant Pinatubo-driven oxygen inventory anomalies for both the upper and deep ocean, with positive anomalies (increased oxygen content with the eruption) in the upper ocean through 1998 (Figure 2d) and lagged changes for the full depth inventory extending for the entire 35 years of this experiment (Figure 2d, Figure S2 in Supporting Information S1). Post eruption, oxygen is immediately absorbed into the upper ocean and then transits to depth quickly where it permanently increases the interior inventory by 60 Tmol (Figure 2d). Globally averaged oxygen concentrations increase by as much as 1 mmol m^{-3} in the upper ocean following the eruption, with anomalies reaching to depths of 250 m in early 1992 and subsequently spreading through the upper kilometer in 1994–1996 (Figure 3b). Anomalies then become insignificant for the global-averaged upper ocean above 250 m, but anomalies at depths greater than 250 m persist for the entire length of the simulation (Figure 3b, and Figure S3 in Supporting Information S1).

Pinatubo-driven anomalies in oxygen inventory exhibit large spatiotemporal variability across the global ocean (Figure 5, left). The oxygen inventory of the upper 1,000 m displays ± 2 mol m^{-2} anomalies in the Northern hemisphere and the tropics in Years 1–3; anomalies in the Southern Ocean do not emerge until Years 3–4 and are concentrated in the Pacific sector (Figure 5, left). Positive anomalies, indicating greater depth-integrated oxygen due to Pinatubo, emerge first in the western boundary current regions of both the North Pacific and Atlantic basins in Year 1 post eruption, where strong ventilation occurs. These anomalies then traverse across the basin with time within the upper 1,000 m, following the mean circulation. In the North Atlantic, subpolar anomalies strengthen from Year 1 to Year 4, concurrent with cool SST anomalies and deeper mixed layer depths in that region (Figure 4). In the North Pacific, increased oxygen inventory is also linked with cool SST and deeper maxMLD anomalies (Figures 4 and 5). The positive anomalies in the North Pacific have only made it half way across the basin by Year 4, but the positive anomalies continue in that same trajectory in Years 5–9 (not shown). In these extratropical regions, Pinatubo-driven cooling, maxMLD deepening, and increased oxygen

Figure 4. Evolution of annual mean anomalies (Community Earth System Model Large Ensemble [CESM-LE] minus CESM-LE-NoPin) sea surface temperature (SST) and maximum mixed layer depth (maxMLD) during the first 5 years following the June 1991 eruption of Pinatubo: Year 0 (July 1991–June 1992), Year 1 (July 1992–June 1993); Year 2 (July 1993–June 1994); Year 3 (July 1994–June 1995); and Year 4 (July 1995–June 1996). SST anomalies are calculated by removing the seasonal cycle and annually averaging over respective months. Positive anomalies (warm colors) indicate warmer temperatures and deeper maximum mixed layer depths with the eruption of Pinatubo. Shading indicates areas without significant difference between the two ensembles at 2σ (Deser, Phillips, Bourdette, & Teng 2012).

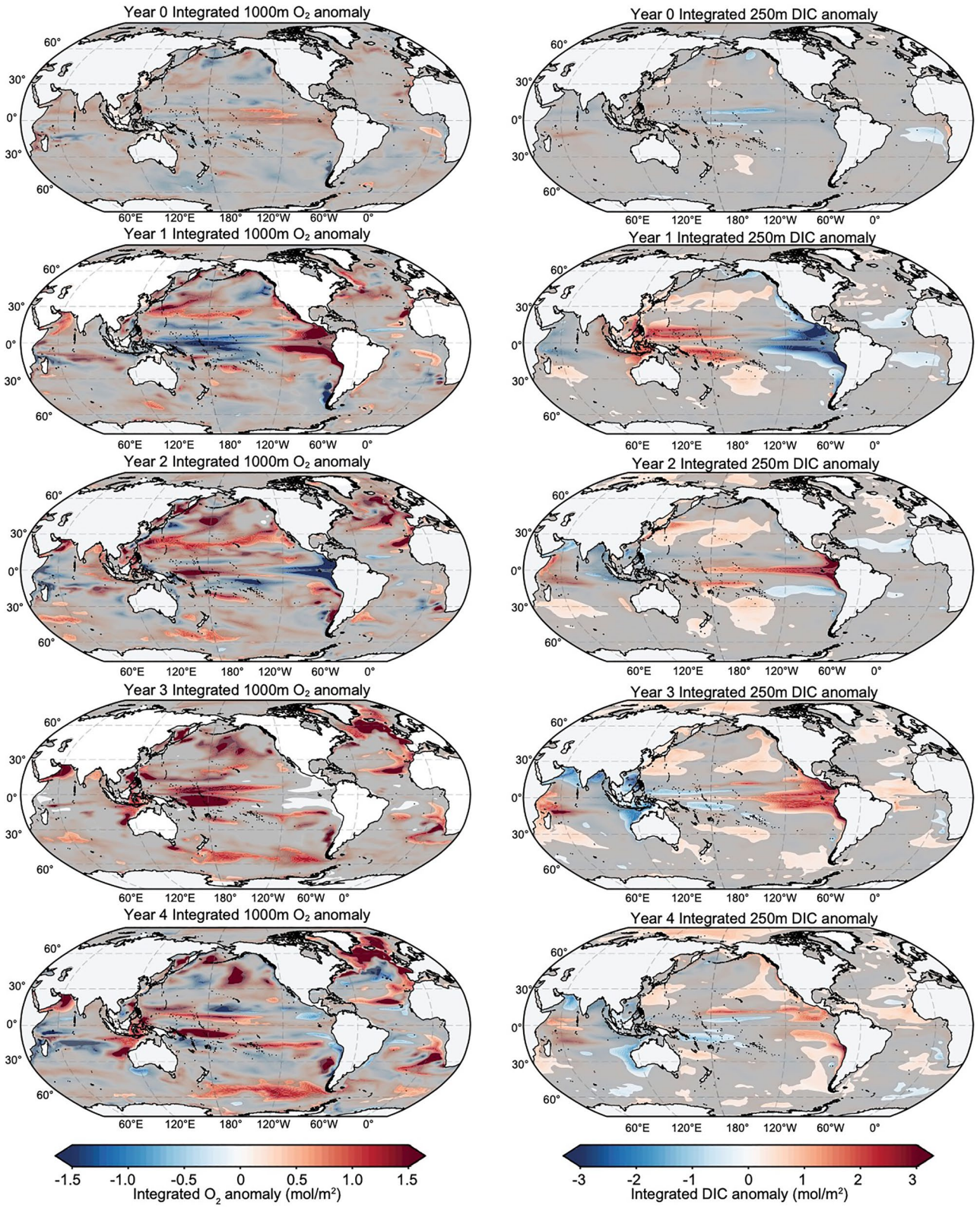
Year 0 Integrated 1000m O2 anomaly
Year 0 Integrated 250m DIC anomaly
Year 1 Integrated 1000m O2 anomaly
Year 1 Integrated 250m DIC anomaly
Year 2 Integrated 1000m O2 anomaly
Year 2 Integrated 250m DIC anomaly
Year 3 Integrated 1000m O2 anomaly
Year 3 Integrated 250m DIC anomaly
Year 4 Integrated 1000m O2 anomaly
Year 4 Integrated 250m DIC anomaly
60°
30°
0°
30°
60°
60°E 120°E 180° 120°W 60°W 0°
-1.5 -1.0 -0.5 0 0.5 1.0 1.5
Integrated O2 anomaly (mol/m²)
-3 -2 -1 0 1 2 3
Integrated DIC anomaly (mol/m²)

Figure 5.

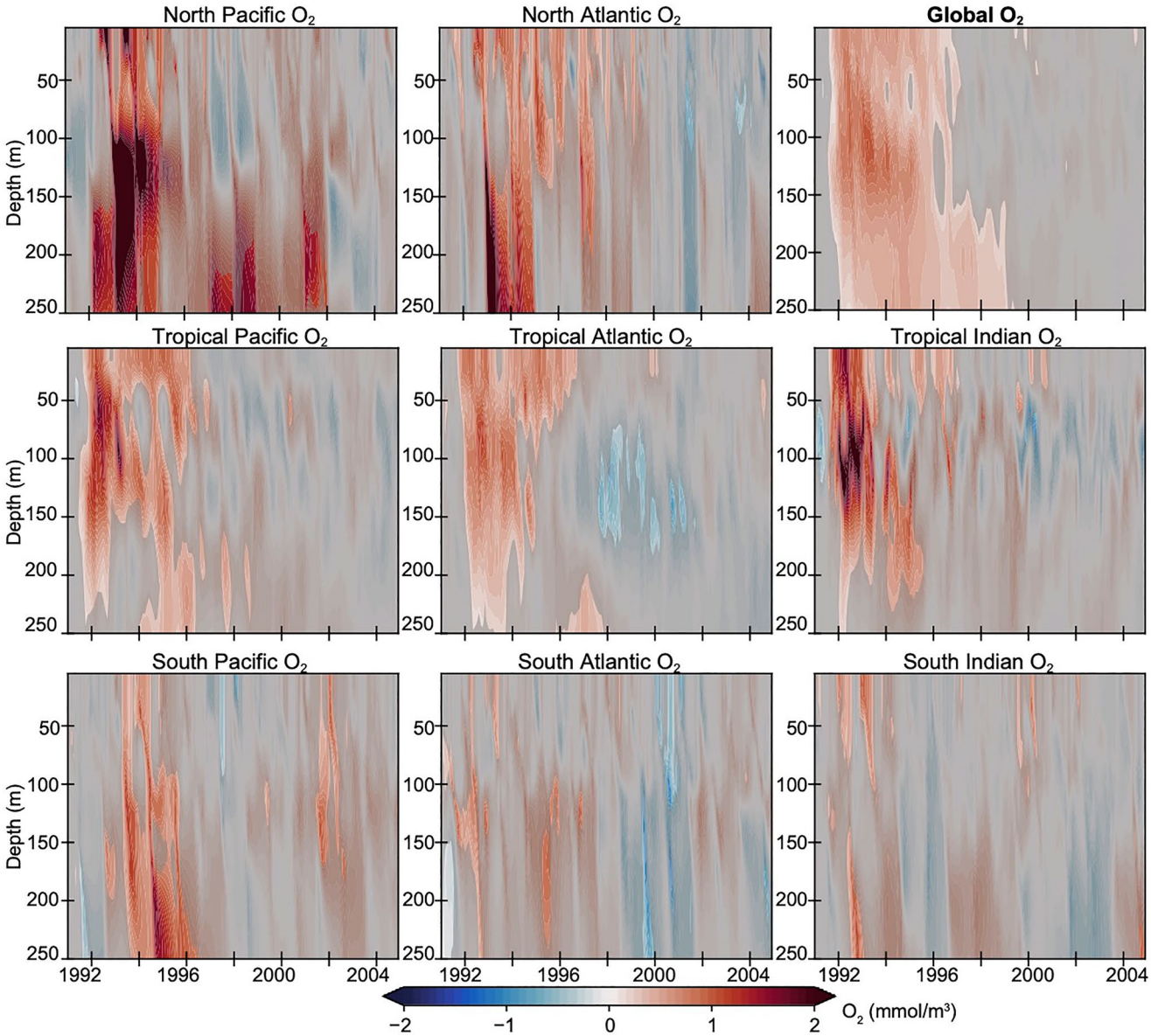

Figure 6. Regionally averaged vertical profile of difference (Community Earth System Model Large Ensemble [CESM-LE] minus CESM-LE-NoPin) plots for ensemble mean O_2 inventory (mmol m^{-3}). Separations are made for the Pacific, Atlantic, and Indian basins into northern (>30°N), tropical (30°N–30°S), and southern sections (<30°S) while the global profile is shown in the top right panel. Shading indicates time/depth where differences are not significant at the 95% confidence level (Deser, Phillips, Bourdette, & Teng 2012). Positive anomalies (warm colors) indicate greater oxygen inventory values with the eruption of Pinatubo while negative anomalies (cool colors) indicate lower oxygen with the eruption. Similar plot with depth extending to 1,000 m is available in Figure S8 in Supporting Information S1.

inventories are consistent with enhanced ventilation. The small regions exhibiting Pinatubo-driven maxMLD deepening correspond to critically important regions for upper ocean oxygenation (Deutsch et al., 2006; van Aken et al., 2011) and drive significant anomalies in the global mean oxygen inventory (Figures 2d and 3b).

Anomalous oxygen due to Pinatubo enters the ocean most quickly in the tropical Indian and Pacific, and quickly penetrates into and below the mixed layer in these basins (Figure 6, Figures S7 and S8 in Supporting

Figure 5. Evolution of annual mean anomalies (Community Earth System Model Large Ensemble [CESM-LE] minus CESM-LE-NoPin) depth integrated O_2 (top 1,000 m) and DIC (top 250 m) concentrations during the first 5 years following the June 1991 eruption of Pinatubo: Year 0 (July 1991–June 1992), Year 1 (July 1992–June 1993); Year 2 (July 1993–June 1994); Year 3 (July 1994–June 1995); and Year 4 (July 1995–June 1996). Anomalies are calculated by removing the seasonal cycle and annually averaging over respective months. Positive anomalies (warm colors) indicate greater depth-integrated O_2 or DIC with the eruption of Pinatubo. Shading indicates areas without significant difference between the two ensembles at 2σ (Deser, Phillips, Bourdette, & Teng 2012).

Information S1). The largest averaged anomalies are found in the North Pacific basin, exceeding 2 mmol m^{-3} for the regional-average anomaly in the upper ocean by 2 years post eruption (Figure 6). In all basins, Pinatubo-driven upper ocean oxygen anomalies exhibit seasonality, consistent with intermittent ventilation in wintertime (Figure 6). Anomalies in the North Pacific persist between 100 and 250 m for over a decade. In the North Atlantic, winter of Year 1 (1992–1993) experiences a ventilation anomaly that also causes anomalies greater than 2 mmol m^{-3} between 100 and 250 m. For multiple years post eruption, wintertime ventilation in the North Atlantic supplies anomalously high oxygen concentrations into the subsurface thermocline (Figure 6, Figure S5 in Supporting Information S1) where oxygen eventually penetrates to depths below 500 m (Figure S8 in Supporting Information S1). This signal also emerges through a strengthening of the Atlantic MOC during the late 1990s due to this increase in ventilation (Figure S10 in Supporting Information S1).

In contrast to the declining oxygen inventory due to ocean warming, Pinatubo-driven anomalies in air-sea CO_2 flux and DIC inventory occur against a background of increasing oceanic CO_2 uptake (Figure 1e) and a steadily increasing DIC inventory (Figure 2e) due to increasing atmospheric CO_2 concentrations prescribed in the modeled atmosphere. The carbon response is associated predominantly with preindustrial carbon, rather than anthropogenic (not shown); all results presented here are for the total carbon. The -0.29 ± 0.14 Pg C yr^{-1} increase in ocean uptake of carbon after the eruption (Figures 1e and 1f) leads to a modest, but statistically significant increase of the ocean DIC inventory of 0.53 Pg C in 1,000 m inventory by 1993 (Figure 2f) with anomalies most pronounced in the upper ocean (0.77 Pg C in the upper 250 m, Figure 2f). In contrast to oxygen inventories that increase with the depth of integration (Figure 2d), Pinatubo-driven anomalies in DIC inventory are largest in the upper ocean integrals and decrease with depth. Therefore the anomalies in the shallow depths and full integral become nearly consistent by 1998 (Figure 2f). This contrast between DIC and oxygen inventory spatial patterns suggests a difference in the processes mediating the generation of anomalies in DIC versus O_2 inventories.

Figure 3c clearly illustrates that the positive anomalies in global-mean DIC are concentrated in the upper 150 m of the ocean during years 1994–1997 (Figure 3c). The slower equilibration timescale for carbon helps to explain the slower DIC response relative to oxygen. Persistent significant anomalies of DIC due to Pinatubo are not detected at depths below 250 m in the global-mean profile, but there are short-lived forced oscillations between significant positive and negative anomalies of smaller magnitude.

Similar to oxygen, we find that Pinatubo-driven DIC anomalies exhibit spatial heterogeneity. For dissolved inorganic carbon inventory (DIC), we focus on the upper 250 m (Figure 5) where the global mean profiles indicate the largest forced response (Figure 3c). Pinatubo's forced excitement of an El Niño event followed by a La Niña event (Figure S4 in Supporting Information S1) is expressed in the upper ocean DIC inventory; the Eastern (Western) Equatorial Pacific exhibits lower (elevated) DIC inventories 1 year post-eruption, while anomalously high DIC inventories can be found in the Eastern Equatorial Pacific during Years 2–3 post-eruption (Figure 5). This DIC anomaly in Year 2–3 is likely also linked to the decrease in carbon efflux occurring in this region during Year 1 (Figure S6 in Supporting Information S1), while the equatorial Pacific DIC inventory anomalies in Year 1 are a reflection of the SST anomalies.

DIC anomalies in the extratropics, from Years 1–3, particularly in the North, also indicate forced increases in the upper ocean DIC content. This is again consistent with increased solubility due to lower annual mean SST in these regions, particularly in Years 1 and 2 (Figure 4, left), that supports increased CO_2 fluxes across the air-sea interface (Figure S6 in Supporting Information S1).

The strongest positive forced anomalies in the upper ocean DIC inventory occur in the northern and tropical Pacific and tropical Indian, with some significant increase in the south Pacific as well (Figure 7, Figure S7 in Supporting Information S1). In the tropical Pacific, circulation anomalies associated with ENSO modify the depth of the thermocline, generating opposite-signed anomalies with depth; the Pinatubo-driven El Niño event leads to decreased DIC in the upper 100 m, while the subsequent La Niña event produces $\sim$>3 mmol m^{-3} increases in upper ocean DIC concentrations (Figure 7). This is in line with the current understanding of how ENSO events impact carbon in this region of the ocean (Eddebbar et al., 2019; Landschützer et al., 2016). A slowdown of the easterlies during typical El Niño events reduces the upwelling of DIC to the surface, driving a reduction in the surface pCO_2, and a reduction of the tropical Pacific carbon flux to the atmosphere.

In the tropical Indian, thermocline oscillations also play a role in the inventory anomalies (Figure 7). In the Northern extratropics, upper ocean DIC anomalies occur several years after the eruption (Figure 7). Unlike oxygen, the additional Pinatubo DIC is concentrated in the upper 100 m and generally does not penetrate to depth (Figure

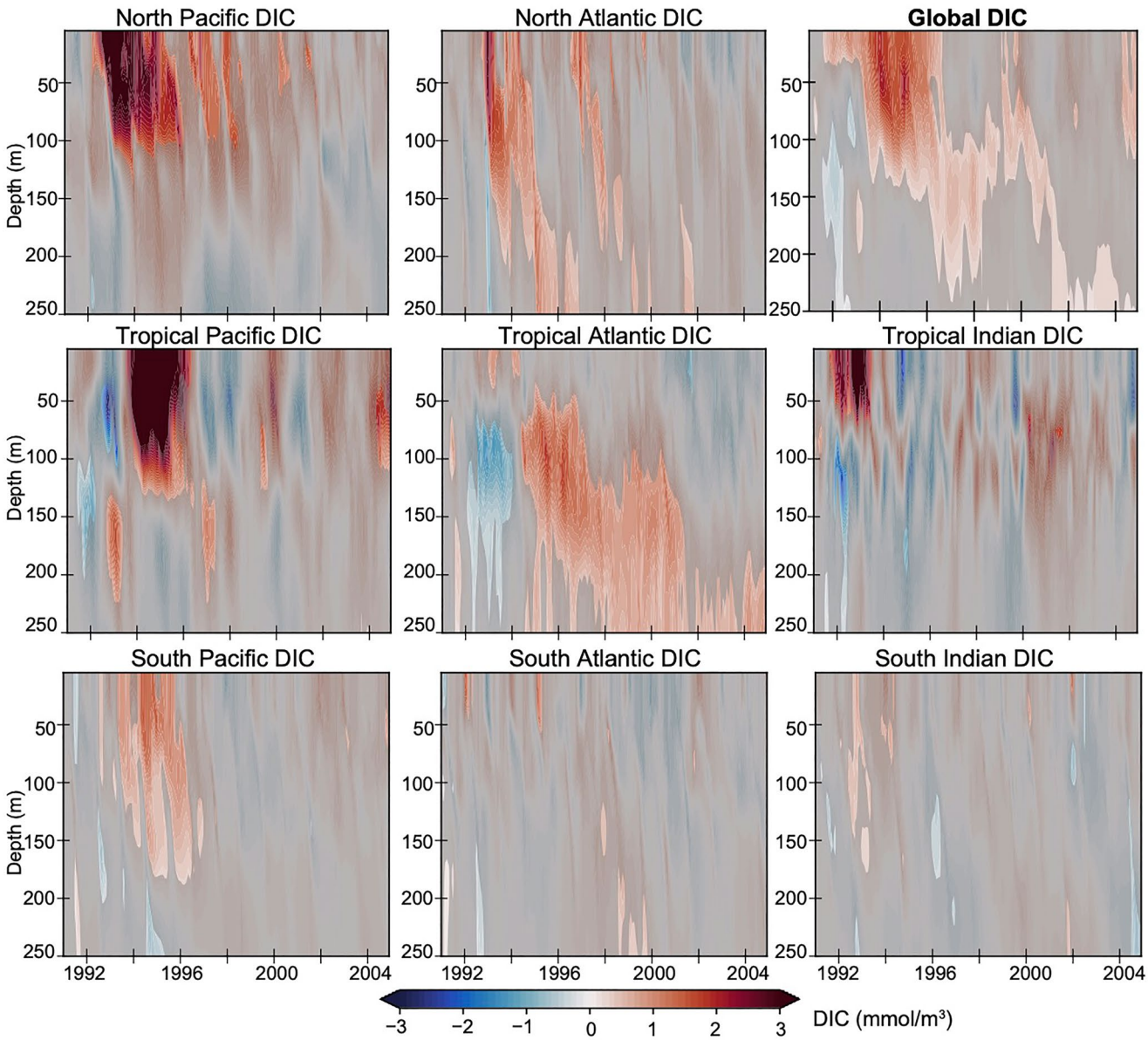

Figure 7. Regionally averaged vertical profile of difference (Community Earth System Model Large Ensemble [CESM-LE] minus CESM-LE-NoPin) plots for ensemble mean DIC inventory (mmol m^{-3}). Separations are made for the Pacific, Atlantic, and Indian basins into northern (>30°N), tropical (30°N–30°S), and southern sections (<30°S) while the global profile is shown in the top right panel. Shading indicates time/depth where differences are not significant at the 95% confidence level (Deser, Phillips, Bourdette, & Teng 2012). Positive anomalies (warm colors) indicate greater DIC inventory values with the eruption of Pinatubo while negative anomalies (cool colors) indicate lower DIC levels with the eruption. Similar plot with depth extending to 1,000 m is available in Figure S9 in Supporting Information S1.

S9 in Supporting Information S1). The exception to this is in the tropical Atlantic which shows a positive DIC anomaly reaching down to below 250 m by 1998 (Figure S9 in Supporting Information S1). Since our division of the regions is made at 30°N, this feature is most likely mode waters that are circulating in the upper subtropical gyre across the 30°N boundary. The positive anomaly persists throughout the length of the simulation at depths between 200 and 400 m (Figure S9 in Supporting Information S1). In the South Pacific south of 30°S, there are modest positive forced anomalies in DIC above 200 m in 1993–1996 (Year 2–4) but the other sectors of the Southern Ocean do not show a similar signal (Figure 7).

Despite clear forced signals in the upper ocean inventories of oxygen and carbon, forced signals in air-sea fluxes are difficult to discern with our model ensemble size (Figures S5 and S6 in Supporting Information S1). Even

with large signals in some regions, forced signals cannot be identified because of the large magnitude of internal variability in surface fluxes (Equation 1). Focusing on DJF-only fluxes (Figures S5 and S6, right in Supporting Information S1) to avoid seasonal cancellation of the signal, does allow for a forced signal to emerge in a few spots (eastern North Atlantic in Year 1 and 3), but on the whole, does not allow a forced signal to be identified throughout much of the surface ocean. Inventories are integrated quantities that damp local internal variability, and allow forced signals to more clearly emerge (Figures 1–3).

Though the flux signals are not statistically identifiable as a forced response at the grid-scale, they do indicate a tendency for increased air-sea exchange of oxygen in North Pacific mode waters in Year 0 and 1 and in the North Atlantic subpolar gyre in Year 2–4 (Figure S5 in Supporting Information S1). DJF anomalies are stronger than annual means in the north, consistent with ventilation being dominantly a wintertime phenomenon. For carbon, the strongest annual mean anomalies occur in Year 1 (negative, increased uptake/less efflux with eruption) and in Year 3 and 4 (positive, reduced uptake/increase efflux with eruption) in the equatorial Pacific, consistent with ENSO variability (Figure S6 in Supporting Information S1). In DJF, there are some patches of significant flux anomalies at subtropical and subpolar latitudes that are mostly negative in Years 0–1 (indicating increased carbon uptake) and then are increasingly positive. These maps support the result that the ocean initially took up more carbon, but then the forced response involved a transition to a state with a reduced sink.

4. Discussion

4.1. Physical Changes With Pinatubo

Our experiments with the CESM-LE allow precise separation of the physical impacts of Pinatubo and their spatio-temporal evolution in the presence of internal variability. Consistent with long-standing knowledge (Church et al., 2005; Eddebbar et al., 2019; Gleckler, AchutaRao, et al., 2006; Gleckler, Wigley, et al., 2006; Marshall et al., 2022; Stenchikov et al., 2009), we find that Pinatubo's eruption caused widespread global cooling, including spatially distinct reductions in SST, localized increases in maxMLD and negative anomalies in upper OHC. The forced surface cooling response, reaching a maximum of 0.18°C, is comparable to observations. NOAA's Optimum Interpolation Sea Surface Temperature (OISST) climate data record shows a global mean SST cooling of 0.12°C with a 4 year recovery time to return to pre-eruption global mean temperatures (Reynolds et al., 2007).

The eruption of Pinatubo generates ENSO variability in CESM (Figure S4 in Supporting Information S1). A forced tendency to El Niño-like conditions emerges about 1 year after the eruption and is followed by La Niña-like conditions in subsequent years (Figure S4 in Supporting Information S1). Over half, or 15 members, of the CESM-LE members develop an El Niño event post-eruption 1992/1993 (DJF), and all of those members develop a strong La Niña event in 1994/1995 (DJF). In contrast, only 7 of the CESM-LE-NoPin ensemble members develop El Niños in 1992/1993, with 6 of them developing a La Niña event in 1994/1995. The significant ENSO response to the Pinatubo eruption in CESM-LE is consistent with other model experiments and paleoproxies that report the emergence of El Niño event in the year following a tropical eruption (Brad Adams et al., 2003; Eddebbar et al., 2019; Khodri et al., 2017; Maher et al., 2015; Ohba et al., 2013; Predybaylo et al., 2017; Stevenson et al., 2017). In the real world, the Pinatubo eruption occurred during a developing El Niño (NOAA, 2019). The limitation of the real world is that it is not possible to directly separate the eruption-driven climatic signal from the phasing of internal climate variability and the background warming trend (Liu et al., 2018). The impacts of ENSO preconditioning prior to a large eruption remain an outstanding challenge for the community studying impacts of volcanic eruptions on the climate system (Marshall et al., 2022; McGregor et al., 2020; Predybaylo et al., 2020; Stevenson et al., 2017; Swingedouw et al., 2017). Though the extent and mechanisms driving this El Niño-like response in models are still debated (McGregor et al., 2020), the subsequent La Niña-like response to Pinatubo identified with these experiments has not been explored.

In contrast to the Pinatubo-driven ENSO response in CESM, the winter (DJF) NAO index has a significant forced response to the eruption for only 1 year during Year 3–4 (1994–1995), while the SAM index does not show a significant forced response to the eruption at any time during the model run (Figure S4 in Supporting Information S1). These results are consistent with previous modeling studies considering strong volcanic eruptions impact on climate signals which found the tendency for NAO to persist in a positive phase over the first post-eruption decade, beginning in Year 3 post-eruption (Zanchettin et al., 2012). For the SAM, McGraw et al. (2016) find that

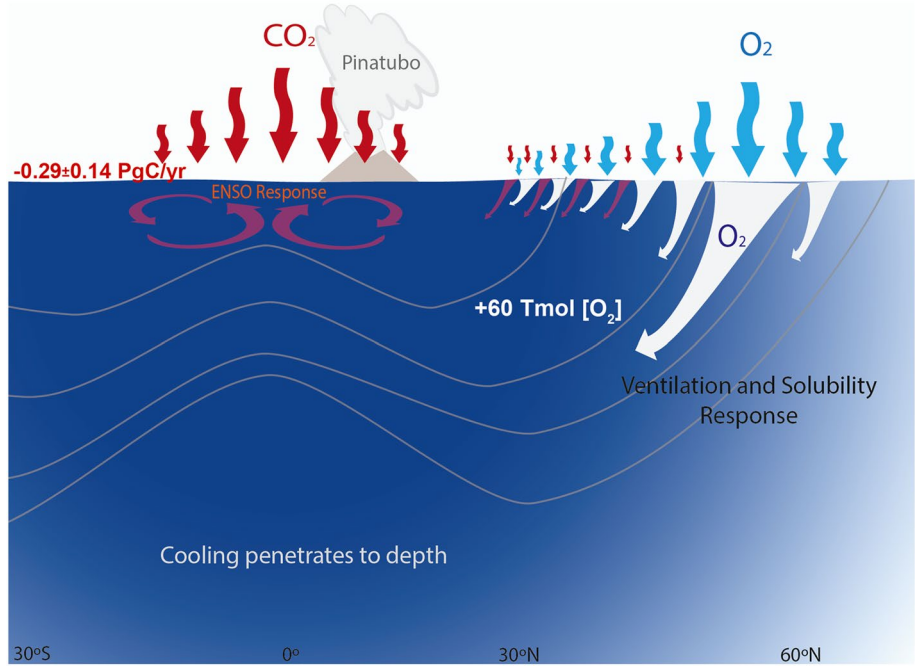

Figure 8. Zonally averaged schematic view of the changes attributable to the eruption of Mount Pinatubo. Ocean cooling is largest in surface layers and low latitudes, but penetrates to depth. Carbon uptake (red arrows) dominates at low latitudes while Oxygen uptake (blue arrows) is predominantly in the mid-latitudes. Oxygen is transported to depth through both ventilation and solubility mechanisms while changes to carbon are dominated by solubility and in response to the ENSO cycle. This model shows an uptake anomaly between the two ensembles of 60 Tmol of Oxygen within 5 years post eruption and a maximum carbon flux increase of −0.29 Pg C yr^{-1} (negative indicating flux into the ocean) 1 year post eruption.

in years following major volcanic eruptions there is a tendency to a more positive median SAM index, however internal variability is large and ENSO state can impact this connection.

Additionally, our results show that Pinatubo forces an increase in the AMOC by 1 Sv (4% of the mean), with individual ensemble members increasing by as much as 5 Sv (20% of the mean) (Figure S10 in Supporting Information S1). This is consistent with previous studies indicating that external forcing from volcanoes has an impact on the overturning circulation (Fang et al., 2021; Swingedouw et al., 2017). The AMOC strengthening found in these CESM anomalies is larger and occurs earlier than that reported by Zanchettin et al. (2012). In their last millennium ensemble results they find an AMOC intensification which culminates roughly one decade after the eruption with anomalies on the order of +0.5 Sv.

4.2. Comparing Pinatubo Impacts on Carbon and Oxygen

Forced carbon and oxygen responses to Pinatubo have quite different spatial patterns (Figures 3 and 5; Figures S5 and S6 in Supporting Information S1), but the globally-averaged temporal evolution is reasonably similar. Oxygen is taken up at higher latitudes and deeper horizons than carbon which is primarily taken up at lower latitudes and further up the water column (Figure 8), in agreement with the findings of Eddebbar et al. (2019). Several aspects of the oxygen and carbon systems help to explain these features.

Oxygen has a much faster air-sea equilibration timescale than carbon, supporting larger and more immediate O_2 fluxes following the eruption. In addition, DIC concentrations increase downward while oxygen decreases with depth in the ocean; when cooling drives deeper mixing it brings up water low in O_2, but high in CO_2. Thus, ventilation promotes greater O_2 fluxes, but dampens CO_2 fluxes, hence the larger O_2 uptake than carbon at higher latitudes.

Both carbon and oxygen fluxes experience an immediate forced global increase in ocean uptake and then a few years later, a rebound to a positive anomaly, or less uptake (Figures 1c–1f). For both gases, the air-sea gradient, $\Delta pX = pX^{atm} - pX^{ocean}$ (with X representing either O_2 or CO_2), sets the magnitude of the flux. Any anomalous

increase in uptake into the surface ocean raises pX^{ocean} and thus reduces the ΔpX such that future fluxes will be damped (Koch et al., 2009; McKinley et al., 2020).

Together, these factors help to explain the larger amplitude anomalies in oxygen fluxes and the deeper penetration of oxygen inventory anomalies. When the surface ocean cools and low oxygen waters are delivered to the surface, oxygen can rapidly be exchanged across the air-sea interface and injected into the deep ocean (Atamanchuk et al., 2020; Körtzinger et al., 2004) (Figures 3 and 6). The window to the surface then closes and the oxygen anomalies are transported at depth (Figure 3).

In contrast, the immediate cooling with Pinatubo primarily increases the carbon carrying capacity by increasing carbon solubility at the surface. Air-sea carbon exchange slowly adds DIC to the ocean and seasonal mixing and mode water formation spreads this anomaly in the upper 150 m. In the tropics, fluxes are modulated by the ENSO cycle, leading to reduced outgassing with the initial post-eruption El Niño, and then additional outgassing with the subsequent La Niña event (Figures S6 and S7 in Supporting Information S1). In the year following Pinatubo, the El Niño response would lead to a slowdown of the easterly winds, which contributes, though only weakly, to reducing the outgassing of carbon, as much of the carbon flux response is driven by changes in surface pCO_2. Outside the tropics, the cooling effects tends to dominate the signal, particularly over the northern mid and high latitudes, where CO_2 is taken up, and thus solubility plays a more dominant role there. The dominance of the El Niño response, which is constricted to the upper ocean, further explains the difference between the O_2 and DIC inventory changes following Pinatubo, whereby O_2 is taken by changes in ventilation and circulation at high latitudes, whereas El Niño effects dominates the CO_2 response. The accumulation of DIC in the upper ocean in the first years after the eruption is concentrated in the North Pacific, Indian, and Southern Ocean (Figure S7 in Supporting Information S1) and this accumulation acts to create a back pressure on fluxes in Years 2–3 after the eruption (Figures 1e, 1f and 5; Figure S6 in Supporting Information S1).

4.3. Pinatubo Impact on Oxygen Fluxes and Inventories

Previous model experiments (Eddebbar et al., 2019; Frölicher et al., 2009) suggest a potentially important role for volcanic eruptions in interrupting ocean deoxygenation and modulating the pronounced interannual-to-decadal variability of the observed ocean oxygen content. The global mean oxygen anomalies forced by Pinatubo, which are isolated in our study, are considerable given current trends measured in the world's ocean. Models predict a decline in the global ocean dissolved oxygen inventory of 1%–7% by the year 2100 (Keeling et al., 2010) and estimate that 55 Tmol per year was lost in the 1990s (Schmidtko et al., 2017). Our model results indicate that the eruption of Pinatubo led to a maximum increase in interior oxygen of about 100 Tmol in the top 1,000 m over the 4 years following the eruption (Figures 2 and 3), more than offsetting the expected deoxygenation for the first half of 1990s and leading to a net increase in the oxygen inventory of about 60 Tmol by the end of the simulation.

Another interesting feature of our results is that oxygen anomalies are decoupled in depth from temperature changes in CESM, suggesting processes such as changes in transport or biogeochemical rates as drivers of oxygen uptake in addition to the solubility effects, as previously suggested by Eddebbar et al. (2019). For example, temperature anomalies are pronounced in upper 0–100 m, while O_2 anomalies are intensified in the 50–200 m depth range (Figure 3). Oxygen changes are also generally more pronounced at depth below 250 m (Figure 2d, Figure S8 in Supporting Information S1), which may offer new insights on the response of ocean circulation to volcanic eruptions. The intensification of the AMOC (Figure S10 in Supporting Information S1) suggests an increase in the advective supply of oxygen to depth as a result of volcanic eruption in the Atlantic basin. Pronounced cooling and a deepened mixed layer at mid and high latitudes likely lead to intensified oxygen uptake and subduction of newly ventilated waters to depth.

4.4. Mechanisms of Air-Sea CO_2 Flux Anomalies With Pinatubo

McKinley et al. (2020) used a simple box model forced with atmospheric pCO_2 and global-mean upper OHC anomalies associated with tropical volcanos to propose a mechanistic explanation for globally integrated air-sea CO_2 flux anomalies since the 1980s. The box model closely replicates ($r > 0.9$) the signals found in ensembles of ocean hindcast models and observation-based pCO_2 products. Based on this evidence, McKinley et al. (2020) proposed a significant role for external forcing from Pinatubo in the variability of the ocean carbon sink in the 1990s.

Here, with CESM-LE, we find a significant forced anomaly of 0.29 Pg C yr^{-1} in the 1992 globally-integrated air-sea CO_2 flux forced by Pinatubo in CESM-LE; and individual members of the ensemble have flux anomalies greater than 0.5 Pg C yr^{-1} (Figures 1e and 1f). CESM-LE also reveals significant spatial structure in the carbon flux and DIC inventory response to the eruption of Pinatubo—the ocean's carbon response to Pinatubo is far from globally uniform (Figures 5 and 7, Figure S6 in Supporting Information S1). In the subtropics and the northern high latitudes, the upper ocean absorbs more carbon, particularly in the subtropics, while ENSO dominates the tropical response (Figures 5 and 7). This heterogeneous spatial response is not at all captured in the box model, yet the box model's CO_2 flux anomaly of 0.5 Pg C yr^{-1} is within a factor of two of the CESM-LE forced response. CESM-LE also indicates a similar forced reduction in the ocean carbon sink in 1994–1995 as in the box model. This feature is consistent with more DIC being held in the upper ocean (Figure 5) where it can raise surface ocean pCO_2 and damp the flux (McKinley et al., 2020) (Figure S6 in Supporting Information S1).

The evolution of the global-mean OHC and global-mean DIC profile (Figure 3) demonstrates the global-mean relationship between upper ocean cooling and DIC content that the box model successfully mimics. The forced change in OHC due to Pinatubo (-3.5×10^{22} J) is within the range estimated from observations and other modeling studies (Church et al., 2005; DeVries, 2022; Eddebbar et al., 2019; Gleckler, AchutaRao, et al., 2006; Gleckler et al., 2016; Stenchikov et al., 2009). The OHC anomaly in the 200 m deep box model of McKinley et al. (2020) is within a factor of two (-5.5×10^{22} J). As in the box model, the globally averaged behavior of CESM-LE is for the negative OHC anomalies to enhance solubility and allow for enhanced air-sea fluxes to persist for long enough (several years) such that additional carbon can be absorbed in the upper ocean (Figure 3). These CESM-LE experiments demonstrate both this global-mean forced response and allow for deeper understanding of the spatially variable mechanisms forced by Pinatubo.

Another study looking at the external forcing of the Pinatubo eruption on the climate system found a cooling of upper ocean (0–300 m) OHC and a subsequent recovery to near zero OHC anomaly by 1996 (DeVries, 2022). However, the models used by DeVries (2022) utilize only historical SST to represent Pinatubo's external forcing in a steady circulation ocean model. Since these SST anomalies impacted only the top model layer of 10 m depth, the resulting globally-integrated OHC anomaly with Pinatubo (-1×10^{22} J) was substantially smaller than most observational studies (Church et al., 2005; DeVries, 2022) and more than three times smaller than the forced response estimated here with CESM-LE. Therefore their resulting small externally forced air-sea CO_2 flux response is consistent with the underestimation of globally-integrated upper ocean cooling and the lack of ENSO response or ventilation changes in a model with steady circulation.

CESM-LE demonstrates a clear CO_2 flux anomaly due to Pinatubo in the global integral (Figures 1e and 1f). But at the local scale, air-sea flux anomalies rarely have a statistically significant forced response (Figure S6 in Supporting Information S1). This is because the large internal variability in surface fluxes obscures the forced signal. This finding is directly comparable to the finding that the air-sea CO_2 flux response to COVID-19 emissions reductions is not detectable at the local scale (Lovenduski et al., 2021). Large internal variability presents a particular challenge to the potential for local flux observations to directly identify climatic signals and argues for continued integration of data into observation-based products from which large-scale signals can be identified (Fay et al., 2021; Fay & McKinley, 2021).

This CESM-LE experiment indicates that the regional centers for CO_2 flux anomalies due to Pinatubo are primarily in the Northern Hemisphere and the tropics, but not in the Southern Ocean (Figure S6 in Supporting Information S1). This contrasts to observation-based products which suggest large amplitude decadal variability in Southern Ocean CO_2 fluxes (Bennington et al., 2012; Hauck et al., 2020; Landschützer et al., 2015) which previous work had linked to the eruption of Pinatubo (McKinley et al., 2020). In-situ sampling (Bakker et al., 2016) in the Southern Ocean may have been too sparse to allow for accurate reconstructions (Gloege et al., 2021) by these products or other mechanisms may be responsible for the observed large amplitude Southern Ocean decadal variability in observation-based products (Gruber et al., 2019). One caveat to this finding comes from the aerosol forcing files used in CESM1 which appear to underestimate aerosol loading in the southern hemisphere (Mills et al., 2016; Neely III et al., 2016; Quaglia et al., 2022). Newer estimates for the aerosol forcing files would likely lead to substantially more cooling and ventilation enhancement in the Southern Ocean, and may lead to more pronounced impacts on carbon fluxes.

With respect to global mechanisms, CESM-LE indicates that the more vigorous overturning of the 1990s, identified by DeVries et al. (2017) as a potential mechanism for ocean carbon sink variability, may have been externally

forced by Pinatubo. Better quantifying the magnitude and mechanisms of CO_2 flux decadal variability globally and in the Southern Ocean is an important focal point for current ocean carbon research.

4.5. Future Work

With this analysis, we have only just begun to explore the impact of the Pinatubo eruption on the ocean and its biogeochemistry. There is much more to be done in terms of understanding the full extent of Pinatubo's impact on ocean physics and biogeochemistry at global, regional, and local scales.

Integrated column inventories and globally integrated fluxes clearly demonstrate the impact of Pinatubo on ocean oxygen and carbon, but locally, significant forced changes in air-sea fluxes are difficult to identify (Figure S6 in Supporting Information S1). Because of the magnitude of internal variability at the surface, future work could expand the number of ensemble members to pinpoint forced changes in surface fluxes.

We highlight here that the Pinatubo effects on ocean biogeochemistry explored in this modeling experiment include the climate impacts of volcanic aerosols on ocean biogeochemistry but do not simulate direct biogeochemical changes associated with increased micronutrient deposition from volcanic ash. Observational studies of smaller eruptions suggest volcanic ash deposition may significantly influence carbon cycling through fertilizing plankton growth at regional scales (Hamme et al., 2010; Langman et al., 2010). The direct biogeochemical contribution of atmospheric deposition of micronutrients by volcanic ash may have additional and complex effects on carbon and oxygen distributions and inventories. These effects are outside the scope of this work, but are worth examining in follow on experiments.

CESM is just one of many Earth system models that have previously generated LENS (Deser et al., 2020). All models are imperfect representations of the real Earth—for example, this version of CESM underestimates Southern Ocean CO_2 uptake (Long et al., 2013) and we do not know if this bias has a role in the small Southern Ocean impacts from Pinatubo that we find here. It would be of great value to have other modeling centers conduct LENS without Pinatubo so that different estimates of forced responses and representation of volcanic aerosol forcings could be compared.

Additionally, work is ongoing to improve the aerosol forcing included by these Earth system models to better capture the observations. Motivated by discrepancies in initial cooling patterns after Pinatubo in CMIP5 models, Neely III et al. (2016) created an improved aerosol forcing file based on updated data sets. For these experiments, CESM-LE had zero aerosol forcing in the Southern Ocean from mid-1991 to mid-1992, and then a forcing that is roughly a 30% underestimated at the peak forcing in late 1992. Newer data sets presented in Quaglia et al. (2022) suggest an approximately symmetric aerosol distribution is more consistent with observations. Such a symmetric aerosol forcing would likely drive a greater carbon and oxygen flux response in the Southern Ocean.

We are currently using the CESM ensembles to investigate the impact of the Pinatubo eruption on hydrographic observations of ocean biogeochemistry (*Olivarez, H.C., Lovenduski, N.S., Eddebbar, Y.A., Fay, A.R., Levy, M., Long, M.C., and McKinley, G.A., The Impact of the Pinatubo Climate Perturbation on Global Ocean Carbon and Biogeochemistry, in preparation for Global Biogeochemical Cycles*) given that the bulk of ocean biogeochemical observations that anchor long-term trends were collected in the years following the Pinatubo eruption through the WOCE/JGOFS (Boyer et al., 2018).

Comprehensive model output is available for scientists to investigate other components of the Earth system, such as the atmosphere, sea ice, and cryosphere.

5. Conclusions

With two initial-condition LENS, we have isolated the impacts of the 1991 eruption of Mt. Pinatubo on the physical and biogeochemical properties of the ocean. Pinatubo forced the ocean to cool to a peak of 0.18°C at the surface and to lose 3.5×10^{22} J of heat. Pinatubo forced an El Ninõ event 1 year after the eruption, and then La Ninã for the two subsequent years. Upper ocean ventilation increased in key regions, allowing for the penetration of oxygen anomalies to depth. These simulations indicate that the long-term effect of Pinatubo on the ocean heat budget was a loss of 2×10^{22} J that persists for multiple decades.

Associated with these physical changes, the ocean absorbed oxygen and carbon, with peak globally integrated forced flux anomalies in 1992 of -42 Tmol O_2 yr^{-1} and -0.29 Pg C yr^{-1}, respectively. In the tropics and northern

high latitudes, the eruption's impact on oxygen is dominated by surface cooling and subsequent ventilation to mid-depths, while the carbon anomaly is associated with solubility changes and eruption-generated ENSO variability (Figure 8). Increased inventories of both gases are found mostly in the tropics and Northern hemisphere, but are very limited in the Southern Ocean. Oxygen anomalies penetrate to the deep ocean, while carbon anomalies remain concentrated in the upper 150 m. For both, full-depth inventories are permanently altered.

Data Availability Statement

The CESM source code is freely available at http://www2.cesm.ucar.edu. The model outputs described in this paper can be accessed at www.earthsystemgrid.org.

Acknowledgments
The authors acknowledge high-performance computing support from Cheyenne (https://doi.org/10.5065/D6RX99HX) provided by NCAR's Computational and Information Systems Laboratory, sponsored by the National Science Foundation (NSF). This material is based upon work supported by the National Center for Atmospheric Research, which is a major facility sponsored by the National Science Foundation under Cooperative Agreement No. 1852977. We are grateful for support from the National Science Foundation (OCE-1948624, OCE-1948664, OCE-1948728, AGS-2019625, OCE 1948599). We acknowledge the previous work done by the CESM Large Ensemble Community Project.

References

Ammann, C. M., Meehl, G. A., Washington, W. M., & Zender, C. S. (2003). A monthly and latitudinally varying volcanic forcing dataset in simulations of 20th century climate. *Geophysical Research Letters*, *30*(12), 1293–1296. https://doi.org/10.1029/2003GL016875

Atamanchuk, D., Koelling, J., Send, U., & Wallace, D. W. R. (2020). Rapid transfer of oxygen to the deep ocean mediated by bubbles. *Nature Geoscience*, *13*(3), 232–237. https://doi.org/10.1038/s41561-020-0532-2

Bakker, D. C. E., Pfeil, B., Landa, C. S., Metzl, N., O'Brien, K. M., Olsen, A., et al. (2016). A multi-decade record of high-quality fCO_2 data in version 3 of the Surface Ocean CO_2 Atlas (SOCAT). *Earth System Science Data*, *8*(2), 383–413. https://doi.org/10.5194/essd-8-383-2016

Bennington, V., McKinley, G. A., Urban, N. R., & McDonald, C. P. (2012). Can spatial heterogeneity explain the perceived imbalance in Lake Superior's carbon budget? A model study. *Journal of Geophysical Research*, *117*(G3), G03020. https://doi.org/10.1029/2011JG001895

Boyer, T. P., Antonov, J. I., Baranova, O. K., Garcia, H. E., Johnson, D. R., Mishonov, A. V., et al. (2018). World Ocean database 2018. In A. V. Mishonov (Ed.), *NOAA Atlas NESDIS 87*.

Brad Adams, J., Mann, M. E., & Ammann, C. M. (2003). Proxy evidence for an El Niño-like response to volcanic forcing. *Nature*, *426*(6964), 274–278. https://doi.org/10.1038/nature02101

Busecke, J. J. M., Resplandy, L., & Dunne, J. P. (2019). The equatorial undercurrent and the oxygen minimum zone in the Pacific. *Geophysical Research Letters*, *46*(12), 6716–6725. https://doi.org/10.1029/2019GL082692

Cabré, A., Marinov, I., Bernardello, R., & Bianchi, D. (2015). Oxygen minimum zones in the tropical Pacific across CMIP5 models: Mean state differences and climate change trends. *Biogeosciences*, *12*(18), 5429–5454. https://doi.org/10.5194/bg-12-5429-2015

Canadell, J. G., Monteiro, P. M. S., Costa, M. H., da Cunha, L. C., Cox, P. M., Eliseev, A. V., et al. (2021). Global carbon and other biogeochemical cycles and feedbacks. In V. Masson-Delmotte, P. Zhai, A. Pirani, S. L. Connors, C. Péan, S. Berger, et al. (Eds.), *Climate change 2021: The physical science basis. Contribution of working group I to the sixth assessment report of the intergovernmental panel on climate change*.

Church, J. A., White, N. J., & Arblaster, J. M. (2005). Significant decadal-scale impact of volcanic eruptions on sea level and ocean heat content. *Nature*, *438*(7064), 74–77. https://doi.org/10.1038/nature04237

Danabasoglu, G., Bates, S. C., Briegleb, B. P., Jayne, S. R., Jochum, M., Large, W. G., et al. (2012). The CCSM4 ocean component. *Journal of Climate*, *25*(5), 1361–1389. https://doi.org/10.1175/jcli-d-11-00091.1

Danabasoglu, G., Lamarque, J. F., Bacmeister, J., Bailey, D. A., DuVivier, A. K., Edwards, J., et al. (2020). The community earth system model version 2 (CESM2). *Journal of Advances in Modeling Earth Systems*, *12*(2), e2019MS001. https://doi.org/10.1029/2019MS001916

Deser, C., Knutti, R., Solomon, S., & Phillips, A. S. (2012). Communication of the role of natural variability in future North American climate. *Nature Climate Change*, *2*(11), 775–779. https://doi.org/10.1038/nclimate1562

Deser, C., Lehner, F., Rodgers, K. B., Ault, T., Delworth, T. L., DiNezio, P. N., et al. (2020). Insights from Earth system model initial-condition large ensembles and future prospects. *Nature Climate Change*, *10*(4), 277–286. https://doi.org/10.1038/s41558-020-0731-2

Deser, C., Phillips, A., Bourdette, V., & Teng, H. (2012). Uncertainty in climate change projections: The role of internal variability. *Climate Dynamics*, *38*(3–4), 527–546. https://doi.org/10.1007/s00382-010-0977-x

Deser, C., Phillips, A. S., Tomas, R. A., Okumura, Y. M., Alexander, M. A., Capotondi, A., et al. (2012). ENSO and Pacific decadal variability in the community climate system model version 4. *Journal of Climate*, *25*(8), 2622–2651. https://doi.org/10.1175/JCLI-D-11-00301.1

Deutsch, C., Brix, H., Ito, T., Frenzel, H., & Thompson, L. (2011). Climate-forced variability of ocean hypoxia. *Science*, *333*(6040), 336–339. https://doi.org/10.1126/science.1202422

Deutsch, C., Emerson, S., & Thompson, L. (2006). Physical-biological interactions in North Pacific oxygen variability. *Journal of Geophysical Research*, *111*(C9), C09S90. https://doi.org/10.1029/2005JC003179

Deutsch, C., Ferrel, A., Seibel, B., Pörtner, H.-O., & Huey, R. B. (2015). Climate change tightens a metabolic constraint on marine habitats. *Science*, *348*(6239), 1132–1135. https://doi.org/10.1126/science.aaa1605

DeVries, T. (2022). Atmospheric co_2 and sea surface temperature variability cannot explain recent decadal variability of the ocean CO_2 sink. *Geophysical Research Letters*, *49*(7), e2021GL096018. https://doi.org/10.1029/2021GL096018

DeVries, T., Holzer, M., & Primeau, F. (2017). Recent increase in oceanic carbon uptake driven by weaker upper-ocean overturning. *Nature*, *542*(7640), 215–218. https://doi.org/10.1038/nature21068

Dutton, E. G., & Christy, J. R. (1992). Solar radiative forcing at selected locations and evidence for global lower tropospheric cooling following the eruptions of El Chichón and Pinatubo. *Geophysical Research Letters*, *19*(23), 2313–2316. https://doi.org/10.1029/92GL02495

Eddebbar, Y. A., Long, M. C., Resplandy, L., Rödenbeck, C., Rodgers, K. B., Manizza, M., & Keeling, R. F. (2017). Impacts of ENSO on air-sea oxygen exchange: Observations and mechanisms. *Global Biogeochemical Cycles*, *31*(5), 901–921. https://doi.org/10.1002/2017GB005630

Eddebbar, Y. A., Rodgers, K. B., Long, M. C., Subramanian, A. C., Xie, S.-P., & Keeling, R. F. (2019). El Niño–like physical and biogeochemical ocean response to tropical eruptions. *Journal of Climate*, *32*(9), 2627–2649. https://doi.org/10.1175/JCLI-D-18-0458.1

Eddebbar, Y. A., Subramanian, A. C., Whitt, D. B., Long, M. C., Verdy, A., Mazloff, M. R., & Merrifield, M. A. (2021). Seasonal modulation of dissolved oxygen in the equatorial Pacific by tropical instability vortices. *Journal of Geophysical Research: Oceans*, *126*(11), e2021JC017567. https://doi.org/10.1029/2021JC017567

Fang, S.-W., Khodri, M., Timmreck, C., Zanchettin, D., & Jungclaus, J. (2021). Disentangling internal and external contributions to Atlantic multidecadal variability over the past millennium. *Geophysical Research Letters*, *48*(23), e2021GL095990. https://doi.org/10.1029/2021GL095990

Fay, A. R., Gregor, L., Landschützer, P., McKinley, G. A., Gruber, N., Gehlen, M., et al. (2021). Seaflux: Harmonization of air–sea CO_2 fluxes from surface pco_2 data products using a standardized approach. *Earth System Science Data*, *13*(10), 4693–4710. https://doi.org/10.5194/essd-13-4693-2021

Fay, A. R., & McKinley, G. A. (2021). Observed regional fluxes to constrain modeled estimates of the ocean carbon sink. *Geophysical Research Letters*, *48*(20), e2021GL095325. https://doi.org/10.1029/2021GL095325

Frölicher, T. L., Joos, F., Plattner, G.-K., Steinacher, M., & Doney, S. C. (2009). Natural variability and anthropogenic trends in oceanic oxygen in a coupled carbon cycle–climate model ensemble. *Global Biogeochemical Cycles*, *23*(1), GB1003. https://doi.org/10.1029/2008GB003316

Frölicher, T. L., Joos, F., & Raible, C. C. (2011). Sensitivity of atmospheric CO_2 and climate to explosive volcanic eruptions. *Biogeosciences*, *8*(8), 2317–2339. https://doi.org/10.5194/bg-8-2317-2011

Frölicher, T. L., Joos, F., Raible, C. C., & Sarmiento, J. L. (2013). Atmospheric CO_2 response to volcanic eruptions: The role of ENSO, season, and variability. *Global Biogeochemical Cycles*, *27*(1), 239–251. https://doi.org/10.1002/gbc.20028

Gleckler, P. J., AchutaRao, K., Gregory, J. M., Santer, B. D., Taylor, K. E., & Wigley, T. M. L. (2006). Krakatoa lives: The effect of volcanic eruptions on ocean heat content and thermal expansion. *Geophysical Research Letters*, *33*(17), L17702. https://doi.org/10.1029/2006GL026771

Gleckler, P. J., Durack, P. J., Stouffer, R. J., Johnson, G. C., & Forest, C. E. (2016). Industrial-era global ocean heat uptake doubles in recent decades. *Nature Climate Change*, *6*(4), 394–398. https://doi.org/10.1038/nclimate2915

Gleckler, P. J., Wigley, T. M. L., Santer, B. D., Gregory, J. M., AchutaRao, K., & Taylor, K. E. (2006). Krakatoa's signature persists in the ocean. *Nature*, *439*(7077), 675. https://doi.org/10.1038/439675a

Gloege, L., McKinley, G. A., Landschützer, P., Fay, A. R., Frölicher, T. L., Fyfe, J. C., et al. (2021). Quantifying errors in observationally based estimates of ocean carbon sink variability. *Global Biogeochemical Cycles*, *35*(4), e2020GB006788. https://doi.org/10.1029/2020GB006788

Gould, J., Sloyan, B., & Visbeck, M. (2013). Chapter 3—In situ ocean observations: A brief history, present status, and future directions. In G. Siedler, S. M. Griffies, J. Gould, & J. A. Church (Eds.), *Ocean circulation and climate, international geophysics* (Vol. 103, pp. 59–81). Academic Press. https://doi.org/10.1016/B978-0-12-391851-2.00003-9

Gruber, N. (2011). Warming up, turning sour, losing breath: Ocean biogeochemistry under global change. *Philosophical Transactions of the Royal Society A*, *369*(1943), 1980–1996. https://doi.org/10.1098/rsta.2011.0003

Gruber, N., Clement, D., Carter, B. R., Feely, R. A., van Heuven, S., Hoppema, M., et al. (2019). The oceanic sink for anthropogenic CO_2 from 1994 to 2007. *Science*, *363*(6432), 1193–1199. https://doi.org/10.1126/science.aau5153

Gupta, M., & Marshall, J. (2018). The climate response to multiple volcanic eruptions mediated by ocean heat uptake: Damping processes and accumulation potential. *Journal of Climate*, *31*(21), 8669–8687. https://doi.org/10.1175/JCLI-D-17-0703.1

Hamme, R. C., Webley, P. W., Crawford, W. R., Whitney, F. A., DeGrandpre, M. D., Emerson, S. R., et al. (2010). Volcanic ash fuels anomalous plankton bloom in subarctic northeast Pacific. *Geophysical Research Letters*, *37*(19), L19604. https://doi.org/10.1029/2010GL044629

Hauck, J., Zeising, M., Le Quéré, C., Gruber, N., Bakker, D. C. E., Bopp, L., et al. (2020). Consistency and challenges in the ocean carbon sink estimate for the Global Carbon Budget. *Frontiers in Marine Science*, *7*, 852. https://doi.org/10.3389/fmars.2020.571720

Holland, M. M., Bailey, D. A., Briegleb, B. P., Light, B., & Hunke, E. (2012). Improved sea ice shortwave radiation physics in CCSM4: The impact of melt ponds and aerosols on Arctic sea ice. *Journal of Climate*, *25*(5), 1413–1430. https://doi.org/10.1175/JCLI-D-11-00078.1

Hunke, E. C., & Lipscomb, W. H. (2008). CICE: The Los Alamos sea ice model user's manual, version 4. In *Los Alamos National Laboratory Technical Report, LA-CC-06-012*.

Hurrell, J. W., Holland, M. M., Gent, P. R., Ghan, S., Kay, J. E., Kushner, P. J., et al. (2013). The community Earth system model: A framework for collaborative research. *Bulletin America Meteorology Social*, *94*(9), 1339–1360. https://doi.org/10.1175/BAMS-D-12-00121.1

Ito, T., & Deutsch, C. (2013). Variability of the oxygen minimum zone in the tropical North Pacific during the late twentieth century. *Global Biogeochemical Cycles*, *27*(4), 1119–1128. https://doi.org/10.1002/2013GB004567

Ito, T., Minobe, S., Long, M. C., & Deutsch, C. (2017). Upper ocean O_2 trends: 1958–2015. *Geophysical Research Letters*, *44*(9), 4214–4223. https://doi.org/10.1002/2017GL073613

Ito, T., Woloszyn, M., & Mazloff, M. (2010). Anthropogenic carbon dioxide transport in the Southern Ocean driven by Ekman flow. *Nature*, *463*(7277), 80–83. https://doi.org/10.1038/nature08687

Kay, J. E., Deser, C., Phillips, A., Mai, A., Hannay, C., Strand, G., et al. (2015). The Community Earth System Model (CESM) large ensemble project: A community resource for studying climate change in the presence of internal climate variability. *Bulletin America Meteorology Social*, *96*(8), 1333–1349. https://doi.org/10.1175/BAMS-D-13-00255.1

Keeling, R. F., Körtzinger, A., & Gruber, N. (2010). Ocean deoxygenation in a warming world. *Annual Review of Marine Science*, *2*(1), 199–229. https://doi.org/10.1146/annurev.marine.010908.163855

Khodri, M., Izumo, T., Vialard, J., Janicot, S., Cassou, C., Lengaigne, M., et al. (2017). Tropical explosive volcanic eruptions can trigger El Niño by cooling tropical Africa. *Nature Communications*, *8*(1), 778. https://doi.org/10.1038/s41467-017-00755-6

Koch, J., McKinley, G. A., Bennington, V., & Ullman, D. (2009). Do hurricanes cause significant interannual variability in the air-sea CO_2 flux of the subtropical North Atlantic? *Geophysical Research Letters*, *36*(7). https://doi.org/10.1029/2009GL037553

Körtzinger, A., Schimanski, J., Send, U., & Wallace, D. (2004). The ocean takes a deep breath. *Science*, *306*(5700), 1337. https://doi.org/10.1126/science.1102557

Landschützer, P., Gruber, N., & Bakker, D. C. E. (2016). Decadal variations and trends of the global ocean carbon sink. *Global Biogeochemical Cycles*, *30*(10), 1396–1417. https://doi.org/10.1002/2015GB005359

Landschützer, P., Gruber, N., Haumann, F. A., Rödenbeck, C., Bakker, D. C. E., van Heuven, S., et al. (2015). The reinvigoration of the Southern Ocean carbon sink. *Science*, *349*(6253), 1221–1224. https://doi.org/10.1126/science.aab2620

Landschützer, P., Ilyina, T., & Lovenduski, N. S. (2019). Detecting regional modes of variability in observation-based surface ocean pCO_2. *Geophysical Research Letters*, *46*(5), 2670–2679. https://doi.org/10.1029/2018GL081756

Langman, O., Hanson, P., Carpenter, S., & Hu, Y. (2010). Control of dissolved oxygen in northern temperate lakes over scales ranging from minutes to days. *Aquatic Biology*, *9*(2), 193–202. https://doi.org/10.3354/ab00249

Lawrence, D. M., Oleson, K. W., Flanner, M. G., Fletcher, C. G., Lawrence, P. J., Levis, S., et al. (2012). The CCSM4 land simulation, 1850–2005: Assessment of surface climate and new capabilities. *Journal of Climate*, *25*(7), 2240–2260. https://doi.org/10.1175/JCLI-D-11-00103.1

Liu, F., Xing, C., Sun, L., Wang, B., Chen, D., & Liu, J. (2018). How do tropical, northern hemispheric, and southern hemispheric volcanic eruptions affect ENSO under different initial ocean conditions? *Geophysical Research Letters*, *45*(23), 13041–13049. https://doi.org/10.1029/2018GL080315

Long, M. C., Deutsch, C., & Ito, T. (2016). Finding forced trends in oceanic oxygen. *Global Biogeochemical Cycles*, *30*(2), 381–397. https://doi.org/10.1002/2015GB005310

Long, M. C., Lindsay, K., Peacock, S., Moore, J. K., & Doney, S. C. (2013). Twentieth-century oceanic carbon uptake and storage in CESM1(BGC). *Journal of Climate*, *26*(18), 6775–6800. https://doi.org/10.1175/JCLI-D-12-00184.1

Lovenduski, N. S., Gruber, N., Doney, S. C., & Lima, I. D. (2007). Enhanced CO_2 outgassing in the Southern Ocean from a positive phase of the Southern Annular Mode. *Global Biogeochemical Cycles*, *21*(2), GB2026. https://doi.org/10.1029/2006GB002900

Lovenduski, N. S., Swart, N. C., Sutton, A. J., Fyfe, J. C., McKinley, G. A., Sabine, C., & Williams, N. L. (2021). The ocean carbon response to COVID-related emissions reductions. *Geophysical Research Letters*, *48*(6), e2020GL092263. https://doi.org/10.1029/2020GL092263

Maher, N., McGregor, S., England, M. H., & Gupta, A. S. (2015). Effects of volcanism on tropical variability. *Geophysical Research Letters*, *42*(14), 6024–6033. https://doi.org/10.1002/2015GL064751

Marshall, L. R., Maters, E. C., Schmidt, A., Timmreck, C., Robock, A., & Toohey, M. (2022). Volcanic effects on climate: Recent advances and future avenues. *Bulletin of Volcanology*, *84*(5), 54. https://doi.org/10.1007/s00445-022-01559-3

McGraw, M. C., Barnes, E. A., & Deser, C. (2016). Reconciling the observed and modeled southern hemisphere circulation response to volcanic eruptions. *Geophysical Research Letters*, *43*(13), 7259–7266. https://doi.org/10.1002/2016GL069835

McGregor, S., Khodri, M., Maher, N., Ohba, M., Pausata, F. S. R., & Stevenson, S. (2020). *The effect of strong volcanic eruptions on ENSO, chapter 12* (pp. 267–287). American Geophysical Union (AGU). https://doi.org/10.1002/9781119548164.ch12

McKinley, G. A., Fay, A. R., Eddebbar, Y. A., Gloege, L., & Lovenduski, N. S. (2020). External forcing explains recent decadal variability of the ocean carbon sink. *AGU Advances*, *1*(2), e2019AV000149. https://doi.org/10.1029/2019AV000149

McKinley, G. A., Fay, A. R., Lovenduski, N. S., & Pilcher, D. J. (2017). Natural variability and anthropogenic trends in the ocean carbon sink. *Annual Review of Marine Science*, *9*(1), 125–150. https://doi.org/10.1146/annurev-marine-010816-060529

McKinley, G. A., Follows, M. J., & Marshall, J. (2004). Mechanisms of air-sea CO_2 flux variability in the equatorial Pacific and the North Atlantic. *Global Biogeochemical Cycles*, *18*(2), C07S06. https://doi.org/10.1029/2003GB002179

McKinley, G. A., Follows, M. J., Marshall, J., & Fan, S.-M. (2003). Interannual variability of air-sea O_2 fluxes and the determination of CO_2 sinks using atmospheric O_2/N_2. *Geophysical Research Letters*, *30*(3), 1101. https://doi.org/10.1029/2002GL016044

McKinley, G. A., Pilcher, D. J., Fay, A. R., Lindsay, K., Long, M. C., & Lovenduski, N. S. (2016). Timescales for detection of trends in the ocean carbon sink. *Nature*, *530*(7591), 469–472. https://doi.org/10.1038/nature16958

Mills, M. J., Schmidt, A., Easter, R., Solomon, S., Kinnison, D. E., Ghan, S. J., et al. (2016). Global volcanic aerosol properties derived from emissions, 1990–2014, using CESM1(WACCM). *Journal of Geophysical Research: Atmospheres*, *121*(5), 2332–2348. https://doi.org/10.1002/2015JD024290

Moore, J. K., Lindsay, K., Doney, S. C., Long, M. C., & Misumi, K. (2013). Marine ecosystem dynamics and biogeochemical cycling in the Community Earth System Model [CESM1(BGC)]: Comparison of the 1990s with the 2090s under the RCP4.5 and RCP8.5 scenarios. *Journal of Climate*, *26*(23), 9291–9312. https://doi.org/10.1175/JCLI-D-12-00566.1

Neely, R. R., III, Conley, A. J., Vitt, F., & Lamarque, J.-F. (2016). A consistent prescription of stratospheric aerosol for both radiation and chemistry in the Community Earth System Model (CESM1). *Geoscientific Model Development*, *9*(7), 2459–2470. https://doi.org/10.5194/gmd-9-2459-2016

NOAA. (2019). National oceanic and atmospheric administration.

Ohba, M., Shiogama, H., Yokohata, T., & Watanabe, M. (2013). Impact of strong tropical volcanic eruptions on ENSO simulated in a coupled GCM. *Journal of Climate*, *26*(14), 5169–5182. https://doi.org/10.1175/JCLI-D-12-00471.1

Predybaylo, E., Stenchikov, G., Wittenberg, A. T., & Osipov, S. (2020). El Niño/Southern Oscillation response to low-latitude volcanic eruptions depends on ocean pre-conditions and eruption timing. *Communications Earth & Environment*, *1*(1), 12. https://doi.org/10.1038/s43247-020-0013-y

Predybaylo, E., Stenchikov, G. L., Wittenberg, A. T., & Zeng, F. (2017). Impacts of a Pinatubo-size volcanic eruption on ENSO. *Journal of Geophysical Research: Atmospheres*, *122*(2), 925–947. https://doi.org/10.1002/2016JD025796

Quaglia, I., Timmreck, C., Niemeier, U., Visioni, D., Pitari, G., Brühl, C., et al. (2022). Interactive stratospheric aerosol models response to different amount and altitude of SO_2 injections during the 1991 Pinatubo eruption. In *Atmospheric chemistry and physics discussions* (pp. 1–35). https://doi.org/10.5194/acp-2022-514

Resplandy, L., Séférian, R., & Bopp, L. (2015). Natural variability of CO_2 and O_2 fluxes: What can we learn from centuries-long climate models simulations? *Journal of Geophysical Research: Oceans*, *120*(1), 384–404. https://doi.org/10.1002/2014JC010463

Reynolds, R. W., Smith, T. M., Liu, C., Chelton, D. B., Casey, K. S., & Schlax, M. G. (2007). Daily high-resolution-blended analyses for sea surface temperature. *Journal of Climate*, *20*(22), 5473–5496. https://doi.org/10.1175/2007JCLI1824.1

Robock, A., & Mao, J. (1995). The volcanic signal in surface temperature observations. *Journal of Climate*, *8*(5), 1086–1103. https://doi.org/10.1175/1520-0442(1995)008¡1086:TVSIST¿2.0.CO;2

Schlunegger, S., Rodgers, K. B., Sarmiento, J. L., Ilyina, T., Dunne, J. P., Takano, Y., et al. (2020). Time of emergence and large ensemble intercomparison for ocean biogeochemical trends. *Global Biogeochemical Cycles*, *34*(8), e2019GB006453. https://doi.org/10.1029/2019GB006453

Schmidtko, S., Stramma, L., & Visbeck, M. (2017). Decline in global oceanic oxygen content during the past five decades. *Nature*, *542*(7641), 335–339. https://doi.org/10.1038/nature21399

Smeed, D. A., Josey, S. A., Beaulieu, C., Johns, W. E., Moat, B. I., Frajka-Williams, E., et al. (2018). The North Atlantic Ocean is in a state of reduced overturning. *Geophysical Research Letters*, *45*(3), 1527–1533. https://doi.org/10.1002/2017GL076350

Smith, R., Jones, P., Briegleb, B., Bryan, F., Danabasoglu, G., Dennis, J., et al. (2010). The Parallel Ocean Program (POP) reference manual, Los Alamos National Laboratory Technical Report LAUR-10-01853, Los Alamos, NM.

Stenchikov, G., Delworth, T. L., Ramaswamy, V., Stouffer, R. J., Wittenberg, A., & Zeng, F. (2009). Volcanic signals in oceans. *Journal of Geophysical Research*, *114*(D16), D16104. https://doi.org/10.1029/2008JD011673

Stevenson, S., Fasullo, J. T., Otto-Bliesner, B. L., Tomas, R. A., & Gao, C. (2017). Role of eruption season in reconciling model and proxy responses to tropical volcanism. *Proceedings of the National Academy of Sciences*, *114*(8), 1822–1826. https://doi.org/10.1073/pnas.1612505114

Swingedouw, D., Mignot, J., Ortega, P., Khodri, M., Menegoz, M., Cassou, C., & Hanquiez, V. (2017). Impact of explosive volcanic eruptions on the main climate variability modes. *Global and Planetary Change*, *150*, 24–45. https://doi.org/10.1016/j.gloplacha.2017.01.006

van Aken, H. M., de Jong, M. F., & Yashayaev, I. (2011). Decadal and multi-decadal variability of Labrador Sea Water in the north-western North Atlantic Ocean derived from tracer distributions: Heat budget, ventilation, and advection. *Deep-Sea Research I*, *58*(5), 505–523. https://doi.org/10.1016/j.dsr.2011.02.008

Wu, X., Okumura, Y. M., DiNezio, P. N., Yeager, S. G., & Deser, C. (2022). The equatorial Pacific cold tongue bias in CESM1 and its influence on ENSO forecasts. *Journal of Climate*, *35*(11), 3261–3277. https://doi.org/10.1175/JCLI-D-21-0470.1

Zanchettin, D., Timmreck, C., Graf, H. F., Rubino, A., Lorenz, S., Lohmann, K., et al. (2012). Bi-decadal variability excited in the coupled ocean–atmosphere system by strong tropical volcanic eruptions. *Climate Dynamics*, *39*(1), 419–444. https://doi.org/10.1007/s00382-011-1167-1